

# American Journal of Science

MARCH 2018

## MOLYBDENUM RECORD FROM BLACK SHALES INDICATES OSCILLATING ATMOSPHERIC OXYGEN LEVELS IN THE EARLY PALEOPROTEROZOIC

DAN ASAE<sup>\*,\*\*,\*†</sup>, OLIVIER ROUXEL<sup>\*,\*\*\*</sup>, SIMON W. POULTON<sup>\*\*\*</sup>,  
TIMOTHY W. LYONS<sup>§</sup>, and ANDREY BEKKER<sup>§</sup>

**ABSTRACT.** The early Paleoproterozoic witnessed Earth's first major oxygenation, referred to as the Great Oxidation Event or GOE. The GOE began around 2.45 billion years ago (Ga) and progressed over hundreds of millions of years, as evidenced by multiple redox indicators, before coming to an abrupt end by *ca.* 2.06 Ga. The details of the GOE and the extent of oxygenation are still not resolved, however, and it is not clear how redox conditions across the GOE compare with those during the middle Proterozoic. In order to investigate the evolution of deep-ocean redox conditions during the GOE, we present Mo concentration and isotope data together with Fe speciation values for three key organic matter-rich shale units of the early Paleoproterozoic age (2.32–2.06 Ga). In addition, we present a new graphical representation of modeling suggesting that the oceanic Mo isotope system is highly sensitive to the balance between anoxic/suboxic and euxinic conditions until deep-ocean oxygenation, similar in scale to modern ocean oxygenation, is reached. Our approach indicates rising, yet oscillating atmospheric oxygen at 2.32 Ga, leading to an abrupt increase in Mo supply to the oceans and large Mo isotope variations under non-steady state conditions. The low seawater  $\delta^{98}\text{Mo}$  value based on the *ca.* 2.32 Ga black shales ( $0.32 \pm 0.58\%$ ) suggests that the oceans were still largely anoxic with locally developed euxinic conditions. Between 2.2 and 2.1 Ga, during the peak of the Lomagundi carbon isotope excursion, we observe higher  $\delta^{98}\text{Mo}_{\text{SW}}$  values ( $1.23 \pm 0.36\%$ ) together with lower Mo concentrations in euxinic shales ( $[\text{Mo}] = 6.3 \pm 9.0$  ppm). We suggest that a decrease in the continental Mo input flux in the later part of the GOE was the main cause of this trend. Lower sulfide availability on the continents after protracted sulfide weathering associated with the early stages of the GOE, and efficient Mo removal in poorly oxygenated oceans under weakly euxinic conditions would both have contributed to the contraction of the Mo oceanic reservoir. By *ca.* 2.06 Ga, the Mo isotope composition of seawater, as inferred from euxinic black shale intervals, became significantly lighter ( $0.70 \pm 0.21\%$ ), reflecting an increased rate of quantitative Mo removal due to the more widespread development of strongly euxinic conditions. Counterintuitively, seawater Mo concentrations recovered, likely due to an increase in the Mo input, which in turn might reflect enhanced weathering of organic carbon-rich shales deposited during the Lomagundi Event.

\* Department of Marine Geosciences, IFREMER, Centre de Brest, 29280 Plouzané, France

\*\* Université de Brest, IUEM, UMR 6538, 29280 Plouzané, France

\*\*\* School of Earth and Environment, University of Leeds, Leeds LS2 9JT, United Kingdom

§ Department of Earth Sciences, University of California, Riverside, California, 92521, USA

§§ Present address: Department of Geology and Geophysics, Yale University, New Haven, Connecticut 06511, USA

§§§ Present address: Department of Oceanography, University of Hawaii, Honolulu, Hawaii 96822 USA

† Corresponding author: Dan Asael (dan.asael@yale.edu)

## INTRODUCTION

It is now widely recognized that Earth experienced a major oxygenation event across the Archean-Proterozoic boundary, referred to as the Great Oxidation Event (GOE; Holland, 2002; Bekker, 2014a). Many lines of evidence support this interpretation (for example, Farquhar and others, 2014; Lyons and others, 2014), including the development of extensive red beds (Cloud, 1968; Roscoe, 1969; Chandler, 1980) and the loss of detrital pyrite and uraninite from the sedimentary rock record (Roscoe, 1969). The absence of mass-independently fractionated (MIF) sulfur in sedimentary pyrite formed after 2.32 Ga (Bekker and others, 2004) provides a minimum age estimate for the Paleoproterozoic sulfur isotope transition, with atmospheric oxygen rising above 0.001 percent of present atmospheric levels (Pavlov and Kasting, 2002). Recent work has focused on clarifying the timing, magnitude and long-term effects of this oxygenation step by focusing on redox conditions shortly before (Anbar and others, 2007; Reinhard and others, 2013; Partin and others, 2013a), during (Kump and others, 2011; Bekker and Holland, 2012; Planavsky and others, 2012a; Canfield and others, 2013; Partin and others, 2013b; Scott and others, 2014; Gumsley and others, 2017; Ossa Ossa and others, 2018) and after (Canfield, 1998; Planavsky and others, 2011) the GOE. The evolving picture of Earth's initial oxygenation now highlights a mildly, likely intermittently oxygenated atmosphere and locally oxygenated ocean surface prior to the GOE (Olson and others, 2013; Lyons and others, 2014), rigorous oxidative weathering of the continents and expansion of the marine sulfate reservoir across the GOE (Planavsky and others, 2012b), and a subsequent crash in surface redox conditions at *ca.* 2.06 Ga (Kump and others, 2011; Scott and others, 2014; Ossa Ossa and others, 2018), prior to the short-lived return of iron formations and then development of widespread low-oxygen conditions by *ca.* 1.85 Ga (Scott and others, 2008; Slack and Cannon, 2009; Poulton and others, 2010; Kendall and others, 2011; Rasmussen and others, 2012).

Here we endeavor to further characterize early Paleoproterozoic redox conditions by combining Mo isotope analyses with Mo concentrations and Fe speciation data for black shales deposited between 2.32 and 2.06 Ga. We focus on three units, each representing a distinct time interval within the early Paleoproterozoic that were previously studied in detail using geochemical and sedimentological techniques to constrain the redox evolution of surface environments (Bekker and others, 2004, 2008; Rouxel and others, 2005; Scott and others, 2008, 2014; Partin and others, 2013a, 2013b; Zerkle and others, 2017; Kipp and others, 2017). These units are the 2.32 Ga Rooihooigte / Timeball Hill formations (THF), the 2.2 to 2.1 Ga Sengoma Argillite Formation (SAF) of South Africa, and the 2.11 to 2.06 Ga Upper Zaogena Formation of Russia.

Our data provide a record of seawater redox conditions in the immediate aftermath of the Paleoproterozoic loss of sulfur MIF, during the peak of the Lomagundi Event (Bekker, 2014b), and immediately following the end of the Lomagundi Event. The primary focus of this study is the isotopic composition of Mo in early Paleoproterozoic seawater, which can provide insight into deep-ocean redox conditions. It has been demonstrated in modern environments that organic matter-rich sediments deposited under highly euxinic conditions (that is, an anoxic, sulfidic water column with  $>11 \mu\text{M H}_2\text{S}$ ) have the potential to record the isotopic composition of contemporaneous seawater (Barling and others, 2001; Arnold and others, 2004; Neubert and others, 2008; Kendall and others, 2009, 2011; Duan and others, 2010; Dahl and others, 2011; Asael and others, 2013). It is important to note that under weakly euxinic conditions, removal of Mo to sediment may be non-quantitative, leading to a significant fractionation of up to 3 permil in the  $^{98}\text{Mo}/^{95}\text{Mo}$  ratio, with the light isotopes concentrated in the sediment (Neubert and others, 2008; Nägler and

others, 2011). Similarly, oxic and suboxic-anoxic (non-sulfidic) conditions are also characterized by large negative Mo isotope fractionations (Poulson and others, 2006; Poulson-Brucker and others, 2009). Hence, the isotopic composition of seawater Mo reflects globally averaged Mo sinks and fluxes controlled by the redox state of the atmosphere-ocean system.

In order to differentiate between euxinic and non-euxinic conditions at the site of deposition we use the Fe speciation technique refined by Poulton and Canfield (2005), which has been employed in numerous Precambrian studies (for example, Reinhard and others, 2009; Poulton and others, 2010; Kendall and others, 2011; Planavsky and others, 2011; Asael and others, 2013; Scott and others, 2014; Thomson and others, 2015). The concentration of Mo in euxinic black shales is known to correlate positively with the concentration of Mo in seawater (Algeo and Lyons, 2006) and thus also provides important information on global sources and sinks of Mo and ocean redox state (Scott and others, 2008).

#### GEOLOGICAL SETTING AND SAMPLE DESCRIPTION

The lower part of the THF was deposited in a deltaic setting of an open-marine basin (Coetzee and others, 2006) between the third and fourth Paleoproterozoic glacial events at *ca.* 2.32 Ga (Hannah and others, 2004). The unit consists of 200-m thick, upward-shallowing cycles, capped by a marine flooding surface, with organic matter-rich and pyritiferous deep-water, pro-delta shales grading upward into delta-front organic matter-lean shales and siltstones and, finally, shallow-water, delta-plain sandstones deposited above the fair-weather wave-base (Coetzee and others, 2006). The unit has experienced only lower-greenschist facies metamorphism. The lower part of the THF sets the minimum age of the GOE as defined by the loss of the S isotope MIF signal (Bekker and others, 2004). It is also the oldest known black shale unit that preserves large mass-dependent S isotope fractionations (MDF; Cameron, 1982; Bekker and others, 2004; Scott and others, 2014; Luo and others, 2016) and thus captures an important transition in Earth's redox state as related to global atmospheric and marine sulfur cycles.

The 2.2 to 2.1 Ga Sengoma Argillite Formation is comprised of up to 700 m of upward-shallowing organic matter-rich and pyritiferous shale, dolostone, chert, siltstone, and fine-grained sandstone that experienced lower-greenschist facies metamorphism. It was deposited in a deep, open-marine setting on the Kaapvaal craton, contemporaneous with the 2.2 to 2.1 Ga Lomagundi carbon isotope excursion (Bekker and others, 2008). The Lomagundi Event refers to a long-lasting positive carbon isotope excursion (with  $\delta^{13}\text{C}$  values typically at, or even higher than, +8‰) preserved globally in sedimentary carbonates (Melezhik and Fallick, 1999). This excursion reflects globally enhanced burial of organic carbon, which could have generated over 20 times the amount of oxygen in the present atmospheric reservoir (Bekker and Holland, 2012 and references therein). Thus, the Lomagundi Event followed the Paleoproterozoic sulfur isotope transition (that is, the loss of MIF in sulfur isotopes) by 100 m.y. and likely represents a much larger increase in Earth's surface oxidation state.

The *ca.* 2.11 to 2.06 Ga Upper Zaogena Formation of the Ludikuvian Series, Russian Karelia, consists of a 1500 m thick sequence of organic matter-rich shales and siltstones, cherts, subordinate dolostones, and basaltic tuffs. It was deposited in a marine basin in the aftermath of the Lomagundi Event (Melezhik and Fallick, 1999) when the marine sulfate reservoir apparently crashed (Scott and others, 2014), likely due to a large-scale de-oxygenation of the atmosphere and ocean. The formation experienced lower-greenschist facies metamorphism.

Since an important aspect of this study is to understand the unique behavior of Mo under euxinic conditions during the GOE and in its immediate aftermath by comparing geochemical data for these three units, all the samples selected for this study are

lithologically similar, organic matter-rich shales. Furthermore, to limit variability in their depositional and diagenetic setting, we sampled only from thick stratigraphic intervals of homogenous, organic matter-rich shales.

#### METHODOLOGY

Powdered samples were ashed in quartz beakers at 600 °C for at least 24 h, and about 200 mg of each sample was dissolved in two steps using mixtures of HNO<sub>3</sub> + HF and HNO<sub>3</sub> + HCl acids. Solutions were then taken up with 20 mL of 7 mol/L HCl. Splits from each sample were taken, evaporated, and brought up in 5 percent HNO<sub>3</sub> for elemental analysis. Molybdenum concentrations were measured using a Thermo Scientific X-series 2 Quad ICP-MS, while Al and Fe concentrations were measured using a Horiba Jobin Yvon Ultima 2 ICP-AES at the Pôle Spectrométrie Océan (UMR 6538), Brest, France. Calibration of the instruments was performed by running a multi-element solution at different concentrations and blank solutions, while standardization was done via measurements of reference materials (BHVO-1, BHVO-2, SDO-1, Nod A-1, and Nod P-1). For the next step, the solutions were doped with Mo double spike and taken through a two-step chromatographic separation following the procedure of Asael and others (2013).

Molybdenum isotope measurements were performed using a Thermo Neptune MC-ICP-MS instrument at the Pôle Spectrométrie Océan (Ifremer), Brest, France. We used a <sup>97</sup>Mo-<sup>100</sup>Mo double-spike solution prepared gravimetrically from Oak Ridge Laboratory metal powders by Asael and others (2013). Optimization of the double-spike isotope composition relative to the SPEX in-house standard gave <sup>95</sup>Mo/<sup>98</sup>Mo, <sup>97</sup>Mo/<sup>98</sup>Mo, and <sup>100</sup>Mo/<sup>98</sup>Mo isotopic ratios of 0.278, 16.663, and 15.704, respectively. Data reduction was performed according to Siebert and others (2001), where iterations were repeated until the difference in the δ<sup>98</sup>Mo value between two consecutive iterations was smaller than 0.001 permil. The typical number of iterations was ≤ 4. Within a given session, standards and samples were measured at a constant concentration. Selected geostandards were processed together with each set of columns resulting in the following values and external precision: Nod-P1 = -0.6 ± 0.10‰ (2SD, n=14); Nod-A1 = -0.44 ± 0.04‰ (2SD, n=11); and SDO-1 = 0.97 ± 0.08‰ (2SD, n=16). The typical standard error of a single measurement (2SE) was 0.05 permil. The MC-ICP-MS machine was operated in a low-resolution mode with an ESI Apex Q introduction system measuring all Mo isotope masses together with <sup>91</sup>Zr and <sup>99</sup>Ru in order to monitor isobaric interferences where correction was never necessary.

Molybdenum isotopic compositions are reported here using the conventional delta notation (in terms of <sup>98</sup>Mo/<sup>95</sup>Mo ratios) relative to the NIST SRM 3134 with the value of +0.25 permil as suggested by Nägler and others (2014). During measurements we used the Mo SPEX standard (Lot 11-177Mo) as a lab standard, where calibration of the SPEX standard relative to NIST-3134 (lot 891307) and Rochester (Lot 802309E) gave:

$$\delta^{98/95}\text{Mo}_{\text{SPEX}} = \delta^{98/95}\text{Mo}_{\text{NIST-3134}} - 0.37 \pm 0.06\text{‰} \text{ (2SD)}$$

$$\delta^{98/95}\text{Mo}_{\text{SPEX}} = \delta^{98/95}\text{Mo}_{\text{Roch}} - 0.05 \pm 0.06\text{‰} \text{ (2SD)}$$

We used the following Fe speciation techniques in order to characterize the redox conditions of the depositional environment. The quantification of pyrite S was determined as described by Canfield and others (1986). Powdered samples were subjected to a hot chromous chloride leach for two hours in order to liberate pyrite S. Sulfide concentrations were determined either via iodometric titration, or gravimetrically following precipitation as Ag<sub>2</sub>S, and converted to pyrite Fe concentrations using the stoichiometry of pyrite (FeS<sub>2</sub>). Unsulfidized highly reactive Fe was quantified using

the sequential extraction technique of Poulton and Canfield (2005), while reactive Fe was quantified via the boiling HCl leach of Berner (1970). Alternatively, we used the traditional approach to determine the degree-of-pyritization (DOP) parameter that was calibrated by Raiswell and others (1994). Highly reactive Fe refers to Fe, which is reactive towards sulfidation on early diagenetic timescales, while reactive Fe additionally includes poorly reactive silicate Fe (Canfield and others, 1992; Poulton and others, 2004), and these two Fe pools are used in the two different Fe-based redox proxies (see below). For the sequential extraction, a separate sample split of approximately 100 mg was subjected to leaching by sodium acetate, sodium dithionite, and ammonium oxalate in order to quantify carbonate Fe (mostly siderite;  $\text{Fe}_{\text{carb}}$ ), ferric oxide ( $\text{Fe}_{\text{ox}}$ ), and magnetite ( $\text{Fe}_{\text{mag}}$ ) pools, respectively. Quantification was accomplished using either an Agilent 5000 quadrupole ICP-MS or by atomic absorption spectroscopy, with a RSD of <5 percent for all stages. Reactive Fe was measured on a leachate derived from boiling approximately 100 mg of sample in concentrated HCl for sixty seconds, with the concentration determined spectrophotometrically. Total organic carbon (after removal of carbonate phases with dilute HCl) and total carbon were measured either on an Eltra C/S elemental analyzer or a Leco C/S elemental analyzer. Total inorganic carbon was calculated as the difference between total carbon and organic carbon.

A subset of 20 samples was analyzed by X-ray diffraction (XRD) to determine mineralogical composition using the Rietveld method, which yields semi-quantitative results. XRD analyses were conducted with a BRUKER AXS D8 Advance machine at IFREMER Institute, Brest, France.

#### RESULTS

The mineralogical compositions determined for the studied sedimentary successions (table 1) are consistent with detrital sources (K-feldspar, plagioclase, quartz, forsterite, and muscovite) and low metamorphic grade as indicated by the presence of chlorite. XRD analyses also show the presence of authigenic minerals (fluorapatite and pyrite), minor oxidation of pyrite during drill-core storage (as indicated by the presence of rhomboclase, szomolnokite, jarosite, and gypsum), and localized hydrothermal alteration in the presence of low- to medium-temperature fluids (for example, pyrophyllite in the THF and, less so, SAF samples). Unreactive Fe mineral phases such as pyroxenes, amphiboles and garnets, which may represent higher metamorphic grade, are not found in our samples.

Our geochemical data are reported in table 2 and are also shown on depth profiles in figure 1. For the sequential Fe extraction we calculate the fraction of Fe considered to be highly reactive ( $\text{Fe}_{\text{HR}}$ ) in the presence of dissolved sulfide (Canfield and others, 1992; Poulton and others, 2004) as  $\text{Fe}_{\text{HR}} = \text{Fe}_{\text{carb}} + \text{Fe}_{\text{ox}} + \text{Fe}_{\text{mag}} + \text{Fe}_{\text{py}}$  (Poulton and Canfield, 2005). Following the criteria of Poulton and Canfield (2011), we identify water column euxinia where the ratio of highly reactive Fe to total Fe ( $\text{Fe}_{\text{HR}}/\text{Fe}_{\text{T}}$ ) is  $> 0.38$  and the ratio of sulfide Fe to highly reactive Fe ( $\text{Fe}_{\text{py}}/\text{Fe}_{\text{HR}}$ ) is  $\geq 0.7$  (fig. 2) (Poulton and Canfield, 2011). The degree of pyritization was calculated as  $\text{DOP} = \text{Fe}_{\text{py}}/(\text{Fe}_{\text{py}} + \text{Fe}_{\text{HCl}})$ . Iron speciation data for SAF and UZF were partially reported in Scott and others (2014).

Average Mo concentrations and Mo/TOC ratios (and total range) are as follows: for the THF,  $[\text{Mo}] = 19.7$  ppm (4.34–67.7 ppm) and  $\text{Mo}/\text{TOC} = 12.5$  (1.6–47.3); for the SAF,  $[\text{Mo}] = 6.3$  ppm (1.35–36.6 ppm) and  $\text{Mo}/\text{TOC} = 0.6$  (0.13–3.3); and for the UZF  $[\text{Mo}] = 25.2$  ppm (1.6–180 ppm) and  $\text{Mo}/\text{TOC} = 2.1$  (0.12–10.8).

Molybdenum isotope values range from  $-0.38$  to  $+1.25$  permil for the THF, from  $+0.00$  to  $+2.21$  permil for the SAF, and from  $+0.16$  to  $+1.83$  permil for the UZF. The samples that were clearly deposited from euxinic bottom waters (as suggested by the Fe-based redox proxies) give average  $\pm$  1SD values of  $\delta^{98}\text{Mo} = +0.32 \pm 0.58$  permil for

TABLE 1  
XRD data

Core	Depth [m]	K-Feldspar (%)	Plagioclase (%)	Quartz (%)	Clay - chlorite (%)	Mica - muscovite (%)	Pyrite (%)					
<b>Core C-175 of the ~2.06 Ga Upper Zaogena Formation (UZF-II) from Karelia, Russia</b>												
C-175	16.60	7	6	44	n.d.	39	4					
C-175	86.90	18	6	57	n.d.	17	2					
C-175	95.30	10	8	67	n.d.	13	2					
C-175	96.90	21	7	57	n.d.	12	3					
C-175	194.80	10	41	33	n.d.	12	4					
C-175	204.30	19	28	37	n.d.	13	3					
<b>Core C-5190 of the ~2.06 Ga Upper Zaogena Formation (UZF-I) from Karelia, Russia</b>												
C-5190	156.00	31	23	33	6	6	1					
C-5190	184.00	18	19	47	5	11	<1					
C-5190	199.00	22	16	57	n.d.	5	<1					
Core	Depth [m]	Dolomite (%)	Plagioclase (%)	Forsterite (%)	Fluorapatite (%)	Quartz (%)	Clay - chlorite (%)	Mica - muscovite (%)	Pyrite (%)	Jarosite (%)	Gypsum (%)	Pyrophyllite (%)
<b>Core Strat 2 of the ~2.15 Ga Sengoma Argillite Formation (SAF) from Botswana</b>												
Strat2	156.70	n.d.	33	<1	n.d.	35	3	21	1	6	n.d.	n.d.
Strat2	173.67	n.d.	24	n.d.	4	38	3	25	3	n.d.	3	n.d.
Strat2	181.25	1	23	n.d.	n.d.	41	4	25	4	n.d.	2	n.d.
Strat2	186.57	n.d.	13	n.d.	n.d.	43	3	28	2	4	n.d.	7
Core	Depth [m]	K-Feldspar (%)	Quartz (%)	Clay - chlorite (%)	Mica - muscovite (%)	Pyrophyllite (%)	Pyrite (%)	Rhombochase (%)	Szomolnokite (%)			
<b>Core EBA-2 of the ~2.32 Ga Timeball Hill Formation (THF) from South Africa</b>												
EBA2	1328.90	2	25	2	63	8	<1	n.d.	n.d.			
EBA2	1338.07	1	41	n.d.	10	n.d.	10	32	6			
EBA2	1338.13	1	74	3	18	1	3	n.d.	n.d.			
EBA2	1338.17	n.d.	47	4	23	<1	12	n.d.	13			
EBA2	1338.20	1	60	3	16	1	9	n.d.	10			
EBA2	1339.00	1	11	2	78	7	<1	n.d.	n.d.			
EBA2	1343.00	1	50	5	37	5	2	n.d.	n.d.			
EBA2	1346.20	2	11	1	54	24	4	n.d.	4			



TABLE 2

Geochemical data. Molybdenum isotope data are reported relative to our internal standard (SPEX) and relative to the NIST 3134 standard  $+0.25\%$  as suggested by Nägler and others (2014). The Fe speciation content of Fe<sub>Carb</sub>, Fe<sub>Ox</sub>, Fe<sub>Py</sub>, and Fe<sub>Meg</sub> represent the extraction steps of Acetate, Dithionite, CrS and Oxalate respectively. DOP is calculated as  $DOP = Fe_{py}/(Fe_{py} + Fe_{HCl})$

Core Name	Depth (m)	$\delta^{98}Mo$ SPEX	$\delta^{98}Mo$ NIST $+0.25$	2se	Mo (ppm)	Mo/TOC	Fe <sub>Cub</sub> wt. %	Fe <sub>Ox</sub> wt. %	Fe <sub>Py</sub> wt. %	Fe <sub>Meg</sub> wt. %	Fe <sub>HCl</sub> wt. %	Fe <sub>HR</sub> wt. %	Fe <sub>T</sub> wt. %	Fe <sub>HR</sub> /Fe <sub>Py</sub> e <sub>HR</sub>	DOP	TOC wt. %	Al wt. %	[Mn] ppm	[Cu] ppm	[U] ppm	[V] ppm	[Zn] ppm	
<b>Core C-175 of the ~2.06 Ga Upper Zaogena Formation (UZF-ID) from Karelia, Russia</b>																							
C-175	16.6	0.69	<b>0.57</b>	0.11	1.6	0.56	0.10	0.12	1.60	0.11	1.04	1.93	3.35	0.58	0.83	0.61	2.88	7.43	51	5	2.0	147	34
C-175	33.7	0.90	<b>0.78</b>	0.12	15.0	1.88	0.05	0.24	4.17	0.06	0.57	4.51	5.00	0.90	0.92	0.88	7.97	4.76	36	67	5.3	289	109
C-175	36.5	0.76	<b>0.64</b>	0.13	44.3	6.41	0.03	0.11	2.32	0.02	0.21	2.48	2.58	0.96	0.93	0.92	6.91	4.87	13	89	5.9	461	86
C-175	38.4	0.62	<b>0.50</b>	0.11	26.0	3.28	0.05		5.97	0.05	0.00	6.06	5.83	1.00	0.98	1.00	7.94	6.47	11	42	12.1	414	147
C-175	54.9	0.79	<b>0.67</b>	0.10	180.2	10.77	0.17	0.03	7.49	0.04	1.73	7.73	7.94	0.97	0.97	0.81	16.73	4.06	43	321	35.7	957	484
C-175	57.3	1.23	<b>1.11</b>	0.10	43.7	3.08	0.14	0.01	6.44	0.01	0.30	6.61	6.44	1.00	0.98	0.96	14.20	3.71	258	169	18.5	414	311
C-175	61.5	0.44	<b>0.32</b>	0.12	35.2	5.34	0.00	0.00	1.65	0.00	0.00	1.66	3.33	0.50	1.00	1.00	6.59	1.20	35	22	7.8	353	63
C-175	70.6	1.95	<b>1.83</b>	0.11	18.0	3.33	0.16	0.01	0.51	0.00	0.47	0.69	2.58	0.27	0.74	0.52	5.40	2.77	25	86	4.9	269	63
C-175	72.6	0.84	<b>0.72</b>	0.12	13.4	1.41	0.00	0.02	1.59	0.00	0.04	1.61	1.55	1.00	0.99	0.98	9.52	4.13	28	187	7.3	399	224
C-175	75.2	0.80	<b>0.68</b>	0.09	5.7	0.86	0.00	0.01	0.92	0.00	0.02	0.94	1.05	0.89	0.98	0.98	6.61	2.54	23	83	1.7	123	124
C-175	80.3	0.89	<b>0.77</b>	0.10	7.4	0.60	0.00	0.01	0.83	0.00	0.00	0.84	0.87	0.96	0.99	1.00	12.43	2.96	24	118	3.3	193	95
C-175	86.9	0.70	<b>0.58</b>	0.09	40.2	1.89	0.02	0.12	0.78	0.00	0.07	0.93	1.38	0.67	0.84	0.92	21.27	3.61	24	400	10.7	587	486
C-175	95.3	0.50	<b>0.38</b>	0.12	107.3	4.83	0.05	0.04	0.88	0.01	0.18	0.98	1.07	0.91	0.90	0.83	22.22	2.50	15	14.9	14.9	864	
C-175	96.9	0.87	<b>0.75</b>	0.13	41.8	1.51	0.04	0.02	1.56	0.01	0.00	1.62	1.57	1.03	0.96	1.00	27.77	3.40	19	572	13.9	687	265
C-175	97.0	0.93	<b>0.81</b>	0.13	15.1	0.89	0.02	0.01	2.12	0.00	0.00	2.16	2.47	0.87	0.98	1.00	16.96	3.81	56	119	4.7	256	558
C-175	98.8	1.05	<b>0.93</b>	0.13	3.2	0.20	0.01	0.07	1.22	0.02	0.05	1.32	1.27	1.00	0.92	0.96	16.30	4.26	30	70	3.6	196	208
C-175	101.5	0.90	<b>0.78</b>	0.12	2.1	0.12	0.03	0.02	1.13	0.02	0.33	1.20	1.35	0.89	0.94	0.77	17.14	4.00	29	48	3.1	222	55
C-175	175.2	0.66	<b>0.54</b>	0.12	13.6	1.32	0.52	0.24	1.61	0.01	4.12	2.38	4.63	0.51	0.68	0.28	10.32	4.91	401	63	4.5	309	145
C-175	176.0	0.79	<b>0.67</b>	0.08	17.7	1.79	0.43	0.27	1.99	0.01	3.33	2.30	3.39	0.68	0.69	0.32	9.90	3.93	173	35	4.5	152	287
C-175	179.4	0.75	<b>0.63</b>	0.10	6.4	0.80	0.54	0.33	1.91	0.01	2.77	2.80	3.99	0.70	0.68	0.41	8.02	5.36	273	6	2.3	212	91
C-175	180.7	0.88	<b>0.76</b>	0.11	4.3	0.91	0.54	0.41	2.36	0.02	3.03	3.33	5.03	0.66	0.71	0.44	4.73	6.94	251	67	1.8	288	124
C-175	194.8	1.23	<b>1.11</b>	0.09	6.5	3.96	0.30	0.03	1.66	0.05	1.03	2.03	3.25	0.63	0.82	0.62	1.64	7.62	116	18	3.4	467	76
C-175	204.3	0.66	<b>0.54</b>	0.12	6.8	0.79	0.03	0.02	1.71	0.03	0.60	1.79	2.98	0.60	0.95	0.74	8.56	6.48	68	171	4.1	250	240

TABLE 2  
(continued)

Core Name	Depth (m)	$\delta^{98}\text{Mo}$ SPEX	$\delta^{98}\text{Mo}$ NIST	2se	Mo (ppm)	Mo/TOC	$\text{Fe}_{\text{C}_{\text{carb}}}$ wt. %	$\text{Fe}_{\text{ox}}$ wt. %	$\text{Fe}_{\text{py}}$ wt. %	$\text{Fe}_{\text{Mag}}$ wt. %	$\text{Fe}_{\text{HCl}}$ wt. %	$\text{Fe}_{\text{HR}}$ wt. %	$\text{Fe}_{\text{T}}$ wt. %	$\text{Fe}_{\text{HR}}/\text{Fe}_{\text{py}}/\text{Fe}_{\text{T}}$ e <sub>HR</sub>	DOP	TOC wt. %	Al wt. %	[Mn] ppm	[Cu] ppm	[U] ppm	[V] ppm	[Zn] ppm	
<b>Core C-5190 of the ~2.06 Ga Upper Zaogena Formation (UZ-F) from Karelia, Russia</b>																							
C-5190	16.0	0.58	0.46	0.09	35.2	1.93	0.01	0.08	0.09	0.16	1.49	0.34	2.04	0.17	0.27	0.06	18.28	4.87	100	219	5.3	586	522
C-5190	78.0	0.84	0.72	0.05	24.2	3.02	0.17	0.02	0.08	0.02	0.73	0.29	3.04	0.10	0.28	0.10	5.93	508	23	2.8	276	78	
C-5190	83.0	1.13	1.01	0.05	13.2	1.41	0.16	0.70	1.31	0.38	2.21	2.55	3.78	0.70	0.51	0.50	9.34	5.01	365	26	2.1	199	221
C-5190	96.0	0.35	0.23	0.10	27.2	1.76	0.12	0.29	0.48	0.30	1.60	1.19	3.49	0.34	0.40	0.23	15.48	4.69	367	48	5.7	424	207
C-5190	100.0	0.47	0.35	0.10	14.5	0.68	0.05	0.25	0.46	0.25	1.19	1.00	2.32	0.43	0.46	0.28	21.34	3.21	216	4	4.1	269	430
C-5190	137.0	0.28	0.16	0.05	13.9	2.11	0.26	0.18	0.09	0.77	5.28	1.30	6.28	0.22	0.07	0.02	6.59	6.28	377	60	2.0	524	77
C-5190	156.0	1.06	0.94	0.08	13.2	1.17	0.09	0.10	0.72	0.15	1.07	1.07	3.03	0.35	0.67	11.30	6.35	64	35	3.8	211	29	
C-5190	184.0	1.04	0.92	0.11	70.7	2.82	0.02	0.07	0.12	0.09	0.62	0.29	1.19	0.24	0.41	0.16	25.11	4.93	66	298	9.0	160	672
C-5190	199.0	0.71	0.59	0.05	27.4	1.10	0.03	0.02	0.19	0.08	0.26	0.33	0.58	0.58	0.59	0.42	25.00	2.39	39	91	4.6	160	672
C-5190	245.0	1.32	1.20	0.11	8.2	0.50	0.20	0.21	0.72	0.38	1.50	1.50	3.72	0.40	0.48	16.48	3.81	267	85	4.5	229	21	
C-5190	292.5	1.57	1.45	0.11	2.0	0.19	0.36	0.19	0.38	0.36	2.55	1.30	4.42	0.29	0.29	0.13	10.40	4.71	537	52	0.8	189	51
C-5190	293.2	1.53	1.41	0.13	1.7	0.20	0.03	0.07	0.24	0.09	0.40	0.43	0.66	0.66	0.55	0.38	8.50	1.29	156	17	0.5	26	4
C-5190	295.6	1.29	1.17	0.10	1.7	0.61	0.55	0.42	0.26	0.68	3.82	1.91	9.70	0.20	0.14	0.06	2.78	8.37	13	0.5	315	105	
<b>Core Strat 2 of the ~2.15 Ga Sengoma Argillite Formation (SAF) from Botswana</b>																							
Strat2	142.8	0.36	0.24	0.05	2.6	0.29	0.00	0.25	0.50	0.71	2.21	0.43	3.35	0.43	0.34	0.18	9.20	8.44	359	35	2.6	124	94
Strat2	156.8	2.33	2.21	0.06	1.9	0.27	0.10	1.23	0.76	0.30	2.36	0.84	2.85	0.84	0.32	0.24	7.10	7.06	251	52	2.7	134	69
Strat2	171.5	1.25	1.13	0.05	1.9	0.19	0.10	0.14	2.01	0.17	0.62	0.90	2.68	0.90	0.83	0.76	10.00	5.91	291	31	3.0	113	99
Strat2	173.7	1.25	1.13	0.04	2.2	0.51	0.06	0.29	2.50	0.02	0.49	0.93	3.08	0.93	0.87	0.84	4.20	7.05	50	38	2.2	101	44
Strat2	177.7	1.31	1.19	0.06	2.0	0.22	0.13	0.08	1.90	0.17	0.47	0.86	2.66	0.86	0.83	0.80	8.90	5.00	427	34	2.8	128	53
Strat2	181.3	1.64	1.52	0.05	2.1	0.27	0.07	0.16	3.02	0.03	0.32	0.91	3.60	0.91	0.92	0.90	7.80	6.91	158	44	3.0	138	106
Strat2	186.6	0.82	0.70	0.05	36.6	3.33	0.24	0.70	2.44	0.07	1.59	0.93	3.72	1.00	0.75	0.61	11.00	6.72	91	55	26.0	86	86
Strat2	200.7	1.61	1.49	0.04	10.9	0.76	0.11	0.11	2.82	0.03	0.34	3.04	3.49	0.87	0.93	0.89	14.40	4.65	318	54	3.3	231	84
Strat2	202.5	1.72	1.60	0.05	6.6	0.43	0.10	0.09	2.73	0.06	0.45	0.92	3.24	0.92	0.92	0.86	15.30	3.45	319	46	4.8	198	76
Strat2	205.3	1.82	1.70	0.04	8.7	0.58	0.10	0.12	2.93	0.02	0.46	1.00	3.15	1.00	0.92	0.86	14.20	4.55	198	48	4.6	182	72
Strat2	209.0	1.63	1.51	0.04	8.8	0.53	0.10	0.16	2.01	0.06	0.59	0.77	3.04	0.77	0.86	0.77	16.60	6.10	265	57	4.1	214	112
Strat2	212.7	0.94	0.82	0.04	4.8	0.34	0.20	0.09	2.10	0.08	0.39	0.91	2.71	0.91	0.85	0.84	14.10	4.60	353	34	3.2	148	60
Strat2	216.8	0.83	0.71	0.06	1.4	0.13	0.10	0.14	1.82	0.34	0.71	1.04	2.30	1.00	0.76	0.72	10.70	4.41	378	34	2.6	133	81
Strat2	238.0	0.12	0.00	0.06	1.5	0.21	0.11	0.05	0.60	0.31	0.00	0.12	4.48	0.12	0.13	7.04	8.41	147	3	3.8	151	55	
Strat2	286.6	1.37	1.25	0.04	2.0	0.13	0.10	0.00	0.60	0.20	1.16	0.25	3.59	0.25	0.67	0.34	15.30	4.87	728	31	1.7	144	67



TABLE 2  
(continued)

Core Name	Depth (m)	$\delta^{98}\text{Mo}$ SPEX	$\delta^{98}\text{Mo}$ NIST	2se	Mo (ppm)	Mo/TOC	Fe <sub>Camb</sub> wt. %	Fe <sub>ox</sub> wt. %	Fe <sub>py</sub> wt. %	Fe <sub>Mag</sub> wt. %	Fe <sub>HCl</sub> wt. %	Fe <sub>HR</sub> wt. %	Fe <sub>T</sub> wt. %	Fe <sub>HR</sub> /Fe <sub>py</sub> F e <sub>HR</sub>	DOP	TOC wt. %	Al wt. %	[Mn] ppm	[Cu] ppm	[U] ppm	[V] ppm	[Zn] ppm
<b>Core EBA-2 of the ~2.32 Ga Timeball Hill Formation (THF) from South Africa</b>																						
EBA2	1327.7	0.15	0.03	0.14	8.9	2.47	0.24	0.35	1.16	0.49	7.76	2.24	7.31	0.31	0.52	0.13	3.59	9.87	155	12.4	107	1024
EBA2	1327.8	-0.25	-0.37	0.12	21.5	7.85	0.00	0.14	0.93	0.73	1.64	1.80	4.61	0.39	0.52	0.36	2.74	11.34	57	8.1	83	431
EBA2	1327.9	0.57	0.45	0.14	7.6	2.22	0.48	0.08	0.70	0.17	5.13	1.43	5.77	0.25	0.49	0.12	3.45	10.86	265	10.0	99	616
EBA2	1328.9	-0.01	-0.13	0.12	6.9	1.61	0.51	0.07	1.00	2.54	2.45	4.12	4.74	0.87	0.24	0.29	4.30	11.35	70	11.2	119	347
EBA2	1338.1	0.04	-0.08	0.04	67.7	47.31	0.99	0.15	6.59	0.02	2.44	7.80	18.37	0.42	0.85	0.73	1.43	1.87	465	71	24.7	63
EBA2	1338.1	0.10	-0.02	0.04	14.9	4.96	0.29	0.06	2.01	0.02	1.12	2.43	2.72	0.89	0.85	0.64	3.01	4.88	155	38	20.6	163
EBA2	1338.2	1.37	1.25	0.04	54.6	20.21	0.49	0.08	6.68	0.04	2.58	7.44	13.42	0.55	0.92	0.72	2.70	5.02	232	227	17.6	185
EBA2	1338.2	0.48	0.36	0.04	20.9	10.93	0.66	0.09	9.03	0.03	1.97	10.04	10.69	0.94	0.92	0.82	1.91	4.37	387	146	39.6	175
EBA2	1339.0	-0.22	-0.34	0.06	4.3	10.58	0.04	0.02	0.14	0.00	0.24	0.20	0.46	0.43	0.71	0.36	0.41	15.74	77	256	12.6	173
EBA2	1343.0	0.83	0.71	0.04	4.4	12.88	0.18	0.04	2.60	0.11	1.40	2.93	5.50	0.53	0.89	0.65	0.34	8.57	232	29	5.5	123
EBA2	1346.2	-0.26	-0.38	0.04	5.5	16.15	0.13	0.04	0.77	0.01	1.24	0.94	5.46	0.17	0.82	0.38	0.34	12.21	77	150	5.6	227

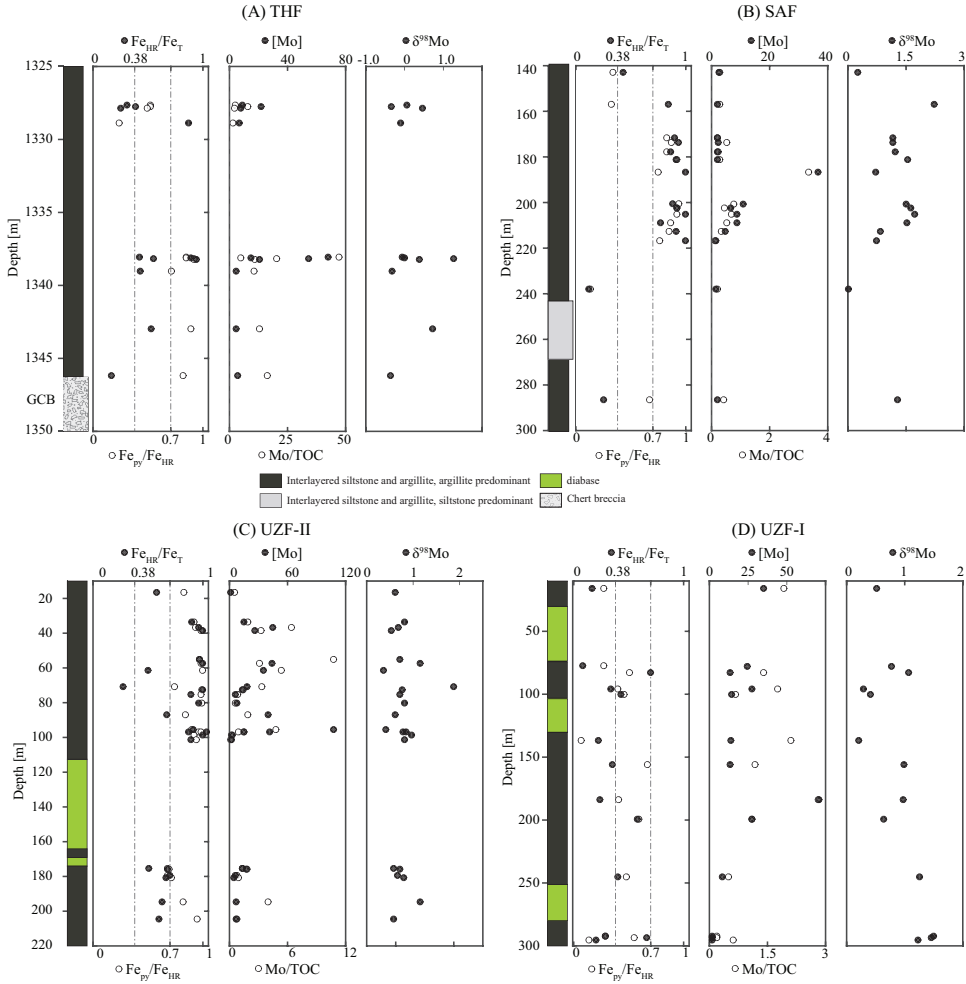


Fig. 1. Chemostratigraphy of the studied units: (A) THF; (B) SAF; (C) UZF-II; and (D) UZF-I. For each sample values of  $Fe_{HR}/Fe_T$ ,  $Fe_{PY}/Fe_{HR}$ , Mo concentrations, Mo/TOC, and  $\delta^{98}Mo$  are plotted against their stratigraphic position (stratigraphic columns are modified from Zerkle and others, 2017; Bekker and others, 2008; and Scott and others, 2014, respectively). Dashed lines in the Fe speciation plots represent the threshold values for euxinia of  $Fe_{HR}/Fe_T > 0.38$  and  $Fe_{PY}/Fe_{HR} > 0.7$ . Filled symbols correspond to the upper axis ( $Fe_{HR}/Fe_T$ , [Mo], and  $\delta^{98}Mo$ ) and open symbols to the lower axis ( $Fe_{PY}/Fe_{HR}$  and Mo/TOC). GCB is the Great Chert Breccia that unconformably underlies the Rooihoogte and Timeball Hill formations.

the THF,  $\delta^{98}Mo = +1.23 \pm 0.36$  permil for the SAF, and  $\delta^{98}Mo = +0.70 \pm 0.21$  permil for the UZF (fig. 3).

DISCUSSION

*Molybdenum Modeling*

In order to better understand the environmental changes potentially captured in the variability we observe in  $\delta^{98}Mo$  values for euxinic samples, we use a simple mass-balance equation modified from Arnold and others (2004) to model the seawater Mo cycle, whereby:

$$f_{IN} \cdot \delta_{IN} = f_O \cdot \delta_O + f_S \cdot \delta_S + f_E \cdot \delta_E \tag{1}$$

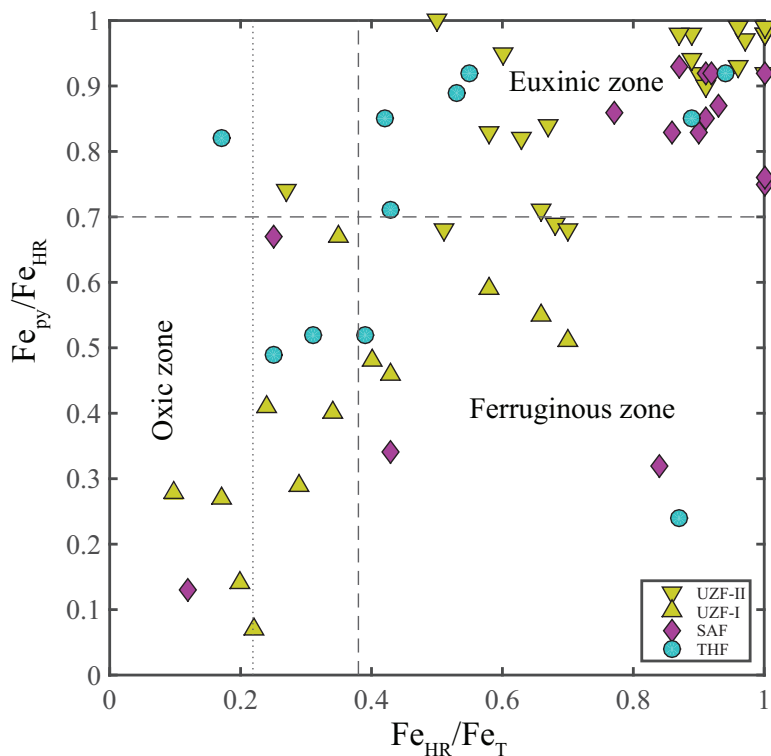


Fig. 2. Iron speciation data for the studied units presented as  $Fe_{HR}/Fe_T$  vs.  $Fe_{py}/Fe_{HR}$ . A euxinic criteria of  $Fe_{HR}/Fe_T > 0.38$  and  $Fe_{py}/Fe_{HR} > 0.7$  as suggested by Poulton and Canfield (2011) was used. Note that euxinic samples are found in each of the studied units.

Here,  $f$  represents the various fluxes into and out of the ocean, and  $\delta$  is the isotopic composition of each flux term. The subscript 'IN' denotes the flux and isotopic composition of the combined riverine and hydrothermal inputs. As described in Asael and others (2013), the isotopic composition of the combined inputs is set at +0.5 permil. This value is slightly lower than the average modern riverine input of 0.7 permil (Archer and Vance, 2008) as we include a hydrothermal input and consider that during long term continental weathering the value should be closer to the crustal average. The subscripts 'O', 'S', and 'E' denote oxidic, anoxic/suboxic, and euxinic sinks, respectively. We use a fractionation factor of  $-3.0$  permil for the oxidic sink based on measurements of modern ferromanganese nodules and crusts (Barling and others, 2001; Barling and Anbar, 2004). Sediments from modern environments with anoxic (but not euxinic) and suboxic water columns have  $\delta^{98}Mo$  compositions that range from  $-0.7$  to  $+1.6$  permil (Poulson and others, 2006). These environments represent a range of bottom-water redox conditions that allow for the recycling of Mn- and Fe-oxyhydroxides in the surface sediments with sulfate reduction restricted to pore waters (Scott and Lyons, 2012). For model purposes we use a fractionation factor of  $-1.0$  permil as an average for Mo removal from seawater to the sediment under anoxic/suboxic conditions. We apply a fractionation factor of 0 permil for highly euxinic environments based on the isotopic composition of modern Black Sea sediments (Arnold and others, 2004). By setting the isotopic composition of the input at +0.5 permil, we can design a three-component diagram that shows contours of  $\delta^{98}Mo_{SW}$  values as a function of any given combination of sink fluxes (fig. 4A).

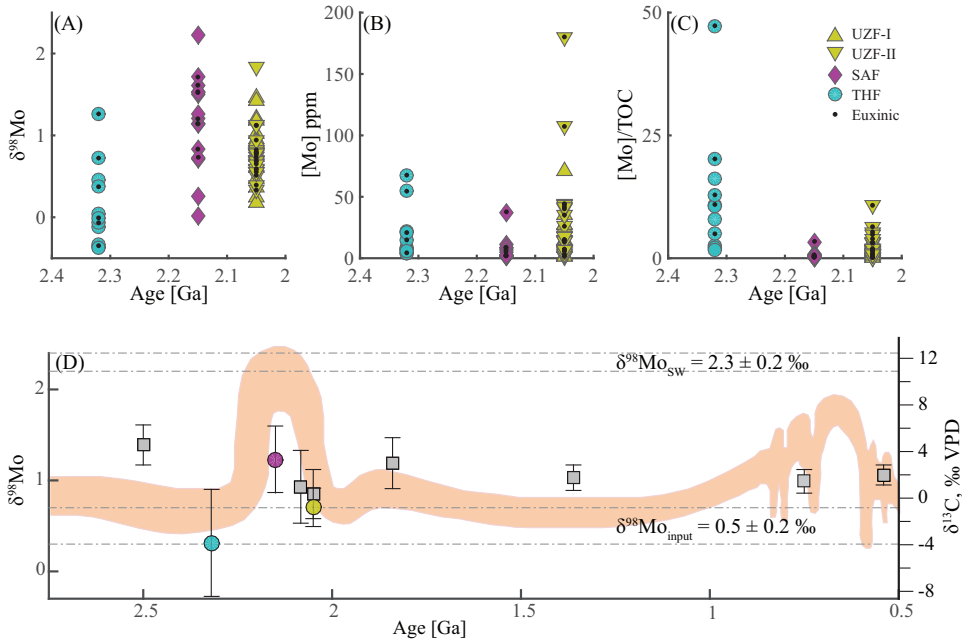


Fig. 3. (A), (B), and (C) show  $\delta^{98}\text{Mo}$ , [Mo], and Mo/TOC values through time, symbols with dots represent euxinic samples. (D)  $\delta^{98}\text{Mo}_{\text{sw}}$  estimates from Late Archean and Proterozoic units (squares denote published data from: Asael and others, 2013 (2.05 Ga); Canfield and others, 2013 (2.08 Ga); Duan and others, 2010 (2.5 Ga); Kendall and others, 2011 (1.85 Ga), 2009 (1.36 Ga); Dahl and others, 2011 (0.75 Ga); and Lehmann and others, 2007 (0.54 Ga), whereas circles denote data from this study. Error bars represent 1 standard deviation of the samples used to calculate the contemporaneous seawater  $\delta^{98}\text{Mo}$  value,  $\delta^{13}\text{C}_{\text{sw}}$  curve from Planavsky and others, 2014 is in the background.

In addition to considering the burial fluxes to each of the three redox-defined settings required to produce the observed  $\delta^{98}\text{Mo}_{\text{sw}}$  values, we can also explore their areal extent. To do so, we rewrite equation 1 as:

$$f_{\text{IN}} \cdot \delta_{\text{IN}} = A_{\text{O}} \cdot B_{\text{O}} \cdot \delta_{\text{O}} + A_{\text{S}} \cdot B_{\text{S}} \cdot \delta_{\text{S}} + A_{\text{E}} \cdot B_{\text{E}} \cdot \delta_{\text{E}} \quad (2)$$

where A is the relative areal extent (that is, fraction of the total seafloor) and B is the Mo burial rate of the oxic (O), anoxic/suboxic (S), and euxinic (E) sinks. Using published burial rates for each sink (Scott and others, 2008), we create a three-component diagram for areal extent (fig. 4B). From this exercise, we find that when  $A_{\text{O}}$  is  $\leq 98$  permil of the seafloor (that is,  $[A_{\text{E}} + A_{\text{S}}] \geq 2\%$  of ocean floor),  $\delta^{98}\text{Mo}_{\text{sw}}$  is almost entirely controlled by the extent of the anoxic/suboxic sink because lines of constant  $\delta^{98}\text{Mo}_{\text{sw}}$  closely follow lines with constant  $A_{\text{E}}/A_{\text{S}}$  ratios in figure 4B. While the oxic sink results in a considerable fractionation from seawater, the burial rate in this setting ( $2 \mu\text{g Mo}/\text{cm}^2 \cdot 10^3 \text{ yr}$ ) is two orders of magnitude lower than in anoxic/suboxic water column environments ( $250 \mu\text{g Mo}/\text{cm}^2 \cdot 10^3 \text{ yr}$ ), where hydrogen sulfide is formed in pore waters (Scott and Lyons, 2012). At the other extreme, euxinic environments are very efficient at removing Mo from seawater with a burial rate of  $1200 \mu\text{g Mo}/\text{cm}^2 \cdot 10^3 \text{ yr}$ . Because Mo removal in euxinic environments is close to 100 percent and, therefore, the net fractionation is essentially 0 permil, it is the expansion and contraction of anoxic/suboxic settings alone that largely controls the  $\delta^{98}\text{Mo}_{\text{sw}}$  values, unless the deep ocean is fully oxygenated, as it is today. An inset of the upper 5 percent of  $A_{\text{O}}$  values (fig. 4C) shows that high  $\delta^{98}\text{Mo}_{\text{sw}}$  values, similar to those found in the modern ocean

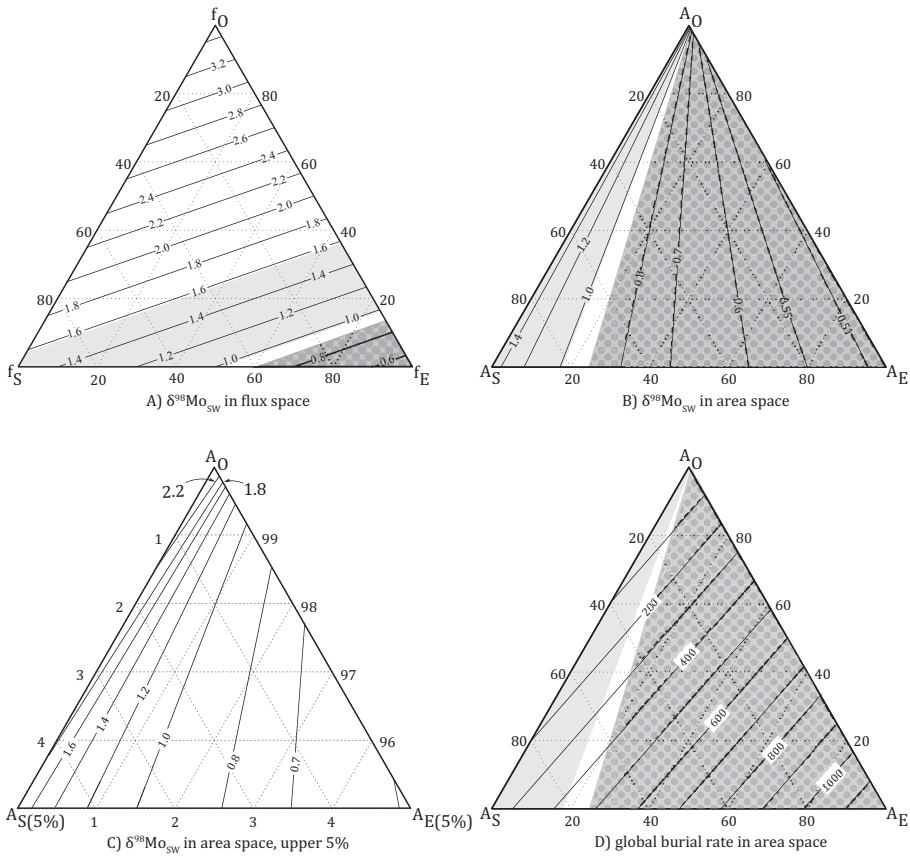


Fig. 4. Three-component diagrams of the Mo seawater isotope system: (A) showing relative fluxes of Mo to redox-different sinks where  $f_O$ ,  $f_E$ , and  $f_S$  represent the Mo fluxes to oxic, euxinic, and suboxic-anoxic sinks, respectively; (B) showing relative seafloor area of the redox-different sinks, where  $A_O$ ,  $A_E$ , and  $A_S$  represent areas of oxic, euxinic, and suboxic-anoxic ocean floor, respectively [based on the average burial rates given in Scott and others (2008)]; (C) an inset of the upper 5% of (B), demonstrating that high  $\delta^{98}\text{Mo}_{\text{SW}}$  values, such as those found in the modern ocean, can only be achieved if the ocean floor is dominated by oxic environments ( $A_O > 98\%$ ); and (D) showing instantaneous, global oceanic Mo burial efficiency in response to a change in the relative sizes of the different redox settings [based on the burial rates given in Scott and others (2008)]. The dotted gray, dark-gray, and pale-gray areas represent the  $\delta^{98}\text{Mo}_{\text{SW}}$  values of the THF, SAF, and UZF, respectively.

( $\delta^{98}\text{Mo}_{\text{SW}} \approx 2.3\text{‰}$ ; Barling and others, 2001; Nägler and others, 2011) are only possible under input parameters used in this scenario in a fully oxygenated ocean when  $A_O \geq 98$  percent.

The burial rates from Scott and others, (2008) were calculated for the modern ocean. However, changes in the seawater Mo concentrations will change the burial rates of the different redox environments in a proportional manner and therefore, will not effect our calculations. For this reason we will use the term burial efficiency in our discussion to represent potentially different absolute burial rate values that at the same time preserve constant ratios between the redox settings.

The considerations above describe the Mo isotope system under ideal conditions. However, the removal of Mo from the seawater to the sediments may deviate from ideal

conditions. Therefore, in the following we show a sensitivity test to this model by changing the net fractionation factors associated with euxinic and anoxic/suboxic environments. First, removal of Mo under euxinic conditions may not always be quantitative, which will result in sediments with  $\delta^{98}\text{Mo}$  values lower than those of the contemporaneous seawater. This may occur in euxinic settings when sulfide concentrations are below the critical threshold required for complete conversion to sulfidized species (Tossell, 2005). For example, net fractionations of  $-0.5 \pm 0.3$  permil are found to occur in the Black Sea, Baltic Sea, and Cariaco Basin between sediments and seawater (Arnold and others, 2004; Neubert and others, 2008; Nägler and others, 2011). Therefore, it might be more realistic to assign a net fractionation factor of  $-0.5$  permil for the removal of Mo in euxinic settings. In addition, in anoxic/suboxic environments where Mo is mostly removed to the sediments through adsorption onto Fe-Mn oxyhydroxides, Mo can be also incorporated into thiomolybdate species where sulfidic pore-waters develop.

In the case of low  $\text{H}_2\text{S}$  levels, where  $\text{Fe}_{\text{py}}/\text{Fe}_{\text{HR}}$  in the sediment is lower than the euxinic threshold, the large fractionation associated with conversion of  $\text{MoO}_4$  to  $\text{MoS}_4$  (up to 6‰; Tossell, 2005) may be in action and would result in more negative  $\delta^{98}\text{Mo}$  values in the sediment. Hence, under anoxic/suboxic conditions a net fractionation factor for Mo removal of *ca.*  $-2$  permil might be a more realistic value. A similar mechanism may work during Mo sorption onto pyrite, where pyrite formation is an important process during diagenesis (Poulson-Brucker and others, 2011). In figure 5 we show another set of three-component diagrams calculated with the above-adjusted values for net fractionation factors in euxinic settings ( $\Delta^{98}\text{Mo}_{\text{SW-SED}} = 0.5\text{‰}$ ) and anoxic/suboxic settings ( $\Delta^{98}\text{Mo}_{\text{SW-SED}} = 2.0\text{‰}$ ). An important difference between these two models is that while under the first set of values the maximum  $\delta^{98}\text{Mo}_{\text{SW}}$  value without a significant oxic sink is *ca.*  $+1.4$  permil, under the second set of adjusted values this ratio increases to about  $+2.4$  permil under the same redox conditions, which is similar to the modern seawater value. Below we discuss geological conditions that could promote each of these two scenarios.

#### *Iron Speciation*

Iron speciation analysis is a common tool for paleoredox reconstructions based on black shales and has been used extensively on Precambrian rocks as old as 2.7 Ga (Reinhard and others, 2009; Planavsky and others, 2011). However, it has been demonstrated that during diagenesis and low-grade metamorphism, unsulfidized, Fe-bearing highly reactive minerals can be transformed to poorly reactive Fe-silicates, lowering  $\text{Fe}_{\text{HR}}/\text{Fe}_{\text{T}}$  and increasing  $\text{Fe}_{\text{py}}/\text{Fe}_{\text{HR}}$  ratios, although this process only tends to be significant when porewater sulfide concentrations are very low (Poulton and others, 2010; Raiswell and others, 2011). Hence, a comparison between the degree of pyritization (DOP) and  $\text{Fe}_{\text{py}}/\text{Fe}_{\text{HR}}$  can help to address the potential for alteration of primary geochemical signals (Cumming and others, 2013). Our data (fig. 6) demonstrate a good correlation between DOP and  $\text{Fe}_{\text{py}}/\text{Fe}_{\text{HR}}$ . Based on this relationship, we are confident that both of the Fe speciation methods represent a primary water column signal. Furthermore, this relationship also demonstrates that poorly reactive Fe-silicates did not form to a significant extent in the three studied units during diagenesis and metamorphism.

Iron speciation analysis of our Paleoproterozoic sample sets identifies both euxinic and anoxic, non-sulfidic (that is, ferruginous) stratigraphic intervals in each of the three studied units and, therefore, may have captured a record of Earth's fluctuating seawater redox conditions from 2.32 Ga to 2.06 Ga. It is important to stress, however, that Fe speciation analysis from a single drill-core only identifies local redox conditions for the time of deposition and cannot be extrapolated to global redox conditions without additional geochemical data (such as Mo isotope compositions) or



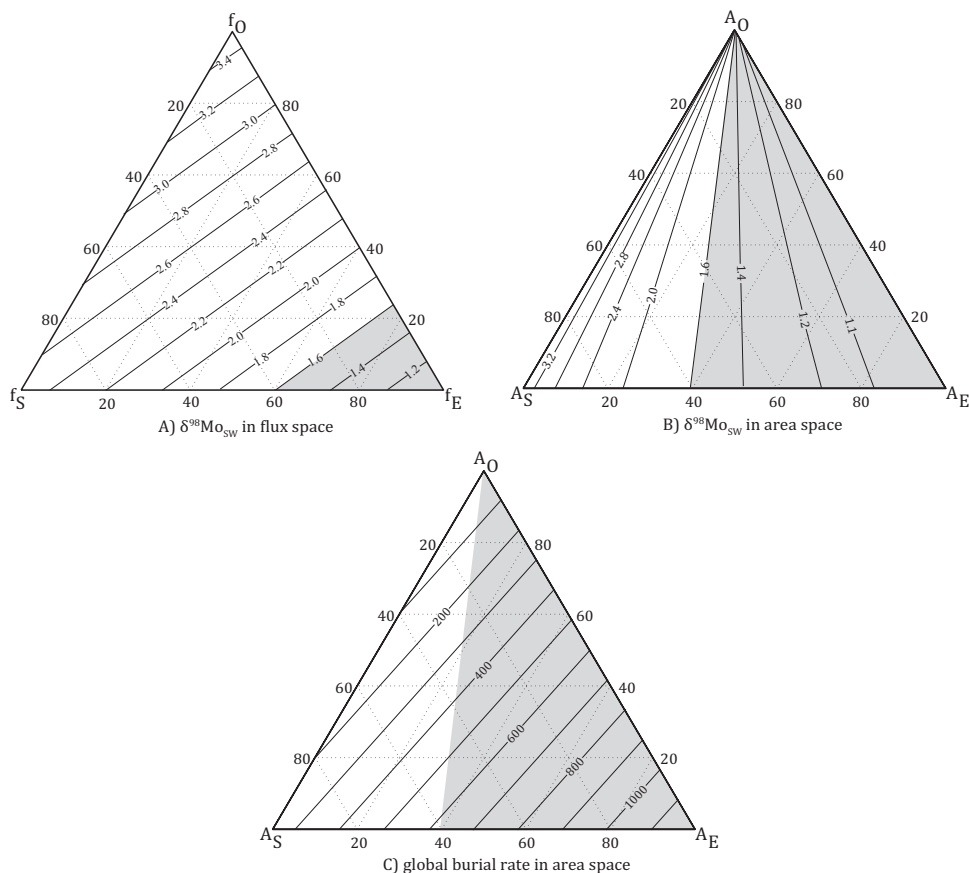


Fig. 5. Three-component diagrams of the Mo seawater isotope system with the adjusted fractionation factors ( $\Delta^{98}\text{Mo}_{\text{SW-SED}} = 0.5\text{‰}$  in euxinic settings and  $\Delta^{98}\text{Mo}_{\text{SW-SED}} = 2.0\text{‰}$  in suboxic-anoxic settings) as discussed in the text: (A) showing relative fluxes of Mo to redox-different sinks where  $f_{\text{O}}$ ,  $f_{\text{E}}$ , and  $f_{\text{S}}$  represent Mo fluxes to oxic, euxinic, and anoxic-suboxic sinks, respectively; (B) showing relative seafloor area of the redox-different sinks, where  $A_{\text{O}}$ ,  $A_{\text{E}}$ , and  $A_{\text{S}}$  represent areas of oxic, euxinic, and anoxic-suboxic ocean floor, respectively [based on the burial rates given in Scott and others (2008)]; and (C) showing instantaneous, global oceanic Mo burial efficiency in response to a change in the relative sizes of the different redox settings [based on the burial rates given in Scott and others (2008)]. The dark-gray area represents the  $\delta^{98}\text{Mo}_{\text{SW}}$  values of the SAF.

a comprehensive study of many other correlative sections worldwide. As shown in figure 2, our THF samples, which were deposited immediately after the Paleoproterozoic loss of sulfur MIF (compare Luo and others, 2016), record euxinic and non-euxinic conditions in approximately equal measure. Our SAF samples, which were deposited during the peak of the Lomagundi Event, show a primarily euxinic signal. Our UZF samples come from two drill cores. The stratigraphically lower core C-5190 (referred here as UZF-I) contains samples deposited under either ferruginous or oxic conditions. In contrast, core C-175 (referred here as UZF-II) primarily records euxinic water column conditions (fig. 2). Previously published pyrite sulfur isotope data from these two cores suggests that the UZF captured a crash in the seawater sulfate reservoir immediately following the end of the Lomagundi Event (Scott and others, 2014).

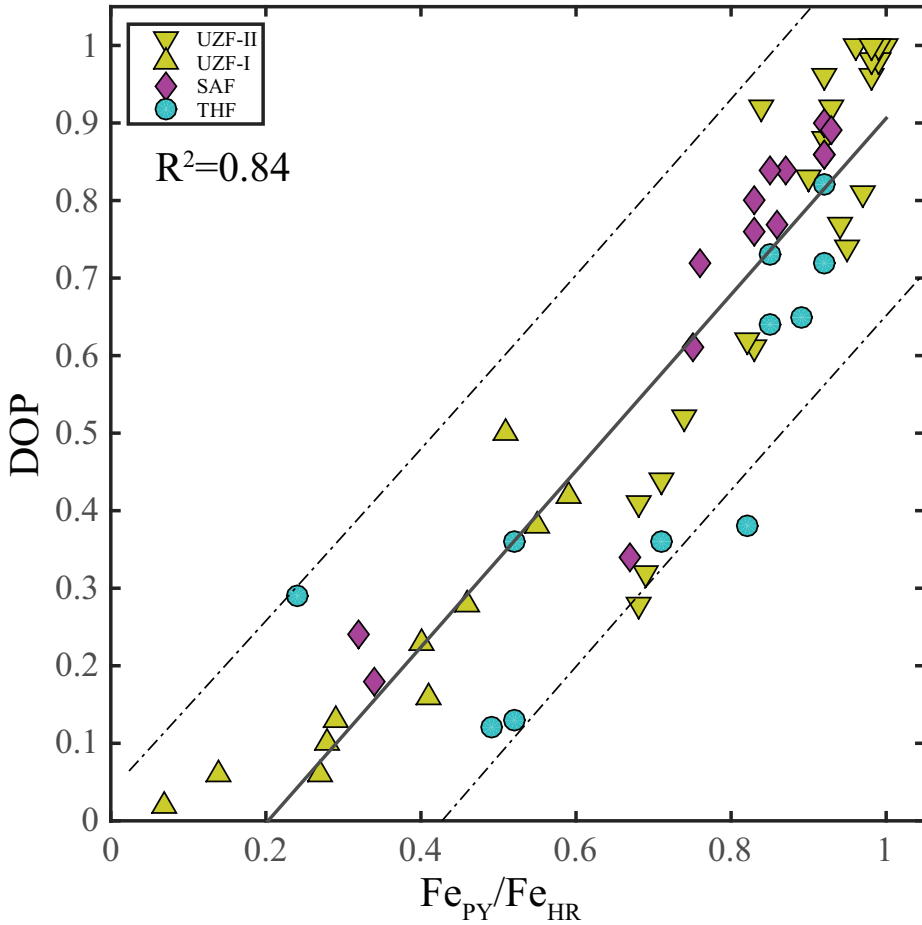


Fig. 6. Correlation between degree of pyritization (DOP) and  $Fe_{PY}/Fe_{HR}$  values for our samples. The solid line represent linear regression where the two dashed lines the 95% confidence level. The good correlation observed between DOP and  $Fe_{PY}/Fe_{HR}$  suggest that both of the Fe speciation methods represent a primary water column signal and that poorly reactive Fe-silicates did not form to a significant extent in the three studied units during diagenesis and metamorphism.

#### *Factors Controlling Molybdenum Enrichment*

The three sedimentary units studied here show elevated Mo/Al ratios of  $1.1 \pm 0.6$  ppm/wt% for the THF,  $1.4 \pm 2.2$  ppm/wt% for the SAF, and  $7.6 \pm 11.6$  ppm/wt% for the UZF, compared to an average of 0.19 ppm/wt% for upper continental crust (Taylor and McLennan, 1995). It should be noted that the THF has a high Al content (up to 12 wt%) relative to the upper continental crust (*ca.* 8 wt%), and thus the Mo/Al ratio likely underestimates the degree to which Mo was enriched from seawater. However, the Mo isotope composition of the three studied formations shows no correlation with Mo concentration or Mo/Al ratio (fig. 7), implying that the Mo in these rocks is predominantly authigenic and that the detrital Mo contribution was negligible. Considering the differences in Mo concentrations, both in the euxinic and non-euxinic samples, among these three units, it is clear that significant changes in oceanic redox conditions, seawater composition, and/or the Mo input fluxes must have occurred during this time interval.

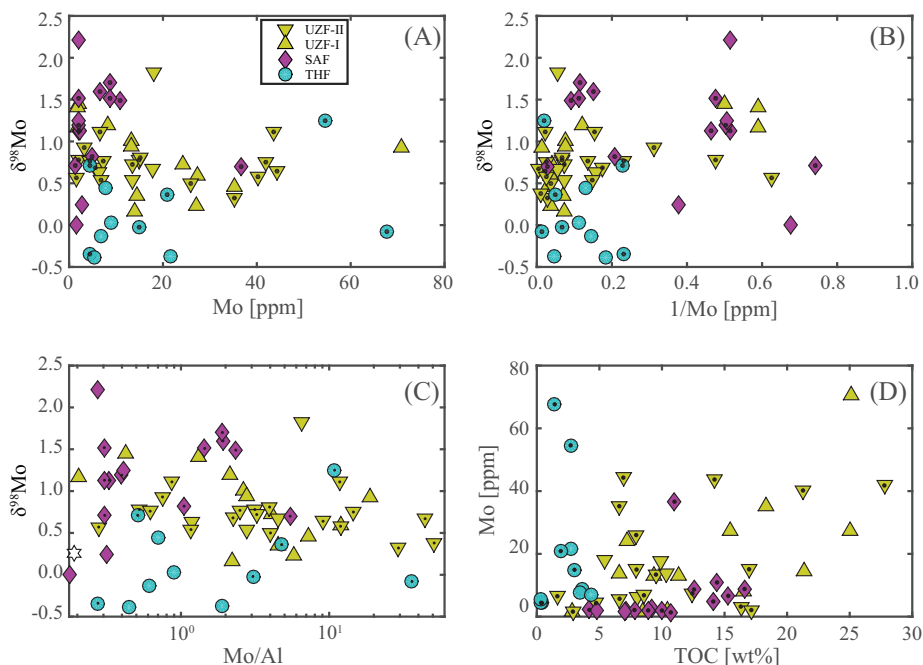


Fig. 7. Molybdenum isotope compositions vs. Mo concentrations (A),  $1/[Mo]$  (B), Mo/Al ratios (C), and Mo concentrations vs. TOC content (D). Dotted symbols represent euxinic samples. Co-variation is not apparent for any of the units on these four plots. The strong co-variation between  $[Mo]$  and TOC content, commonly observed for Phanerozoic black shales (for example, Algeo and Lyons, 2006), is also not apparent in our early Paleoproterozoic data.

The concentration of Mo and the ratio of Mo to total organic carbon (Mo/TOC) in euxinic black shales have been shown to track the concentration of Mo in the overlying water column (Algeo and Lyons, 2006). Furthermore, the concentration of Mo in seawater is thought to reflect both the oxidative weathering flux from the continents and the extent of oxic, suboxic, and euxinic oceanic settings due to differences in burial efficiencies in each of these environments (Scott and others, 2008). Thus, it is important to consider Mo concentrations and Mo/TOC ratios in concert with  $\delta^{98}Mo$  values. The average concentration of Mo in euxinic samples from the THF, SAF, and UZF are  $27.8 \pm 26.9$  ppm,  $7.8 \pm 10.14$  ppm, and  $31.6 \pm 44.1$  ppm, respectively. The Mo concentrations and Mo/TOC ratios show a similar trend with time, with the lowest values observed in the SAF (fig. 3). The observed pattern of Mo concentrations could also be a result of differences in sedimentation rates between the three units. However, the uniform lithology, redox conditions (euxinic) and burial efficiency, together with the fact that Mo/TOC ratios also show the same pattern between the three studied units, suggests that different sedimentation rates were not an important factor. The co-variation between Mo concentrations and TOC that is conspicuous in many Phanerozoic black shale units (Algeo and Lyons, 2006), but also in the 2.5 Ga Mt. McRae shale (Anbar and others, 2007), is not observed in our early Paleoproterozoic black shales (fig. 7C), suggesting secular variations in the Mo seawater concentration.

Since Mo isotopes are most strongly fractionated in oxic environments where Mo burial efficiencies are low, and Mo net isotope fractionations are smallest under euxinic conditions where Mo burial efficiencies are highest, it is expected that for a given Mo input flux, low  $\delta^{98}Mo_{SW}$  values will correlate with low seawater Mo concentra-

tions and therefore lower Mo concentrations in black shales. Consistent with this argument, in figure 4D we calculated instantaneous, global oceanic Mo burial efficiencies in response to a change in the relative sizes of the different redox settings. By comparing figures 4B and 4D one can see that an increase in the areal extent of euxinic environments would result in a decrease in the  $\delta^{98}\text{Mo}_{\text{SW}}$  value and, at the same time, an increase in the average global burial efficiency. Consequently, once steady-state is re-established, lower [Mo] in seawater and in associated euxinic black shales will occur.

However, such a correlation is not observed in our dataset. For the SAF we observe  $\delta^{98}\text{Mo}$  values higher than those for both the THF and UZF, possibly reflecting the expansion of oxic and suboxic-anoxic environments at the expense of euxinic environments. Consistent with this interpretation, an increase in seawater sulfate content is inferred during the Lomagundi Event (Planavsky and others, 2012a; Scott and others, 2014). The expansion of oxic and suboxic-anoxic environments should have resulted in higher seawater Mo concentrations and higher Mo contents in euxinic shales of the SAF. In contrast, we observe low Mo concentrations in euxinic shales of the SAF. Conversely, euxinic shales of the UZF show low  $\delta^{98}\text{Mo}_{\text{SW}}$  values, but higher Mo concentrations compared to the SAF. These observations suggest that other factors (in addition to ocean redox changes), such as variations in the Mo riverine flux and organic carbon burial on a local scale, as well as seawater sulfate content, could have influenced Mo isotope composition and concentration in Paleoproterozoic seawater. These issues will be discussed further in the next section.

#### *Molybdenum Isotope Variations and Inferred Seawater Values*

To summarize, the Mo isotope composition of modern sediments deposited under euxinic conditions is known to approach or match that of seawater. For example, sediments from the euxinic Cariaco Basin and highly euxinic Black Sea have bulk isotopic compositions of +1.8 permil and +2.3 permil, respectively, comparable to a seawater composition of +2.3 permil (Arnold and others, 2004; Neubert and others, 2008; Nägler and others, 2011). The isotopic composition of modern seawater is significantly enriched relative to that of the average of the riverine and hydrothermal sources (+0.5‰; Asael and others, 2013), which is due to adsorption of the molybdate ion ( $\text{MoO}_4^{2-}$ ) onto Mn- and Fe-oxhydroxides under widespread oxic conditions in the modern ocean, a process that is associated with a fractionation factor of  $\Delta^{98}\text{Mo}_{\text{SW-OXIC}} \approx 3\text{‰}$  (Barling and others, 2001; Barling and Anbar, 2004; Goldberg and others, 2009). Thus, as the global extent of oxic and suboxic-anoxic conditions expands and contracts, the Mo isotope composition of seawater changes, and this signal may be captured in contemporaneous euxinic environments. Under globally euxinic conditions, where mechanisms for Mo removal are associated with smaller net fractionations, the isotopic composition of seawater will approach that of the riverine source. Based on these considerations, the Mo isotopic composition in euxinic black shales has been used to estimate the global redox state of the ancient oceans (Arnold and others, 2004; Lehmann and others, 2007; Duan and others, 2010; Dahl and others, 2011; Kendall and others, 2011; Asael and others, 2013). Kendall and others (2011) demonstrated that during the Paleoproterozoic the oceans were isotopically homogenous with respect to Mo. An estimate of the seawater  $\delta^{98}\text{Mo}$  value based on Paleoproterozoic sediments deposited in euxinic settings can therefore provide a paleoredox proxy for the global contemporaneous ocean.

It is important to note that even though the oceans were generally homogenous with respect to Mo, local, short-term fluctuations in Mo isotope composition of seawater may have still occurred at the sites of sedimentation. Such fluctuations could have resulted from Rayleigh distillation effects and local, non-quantitative Mo removal, which may drive the sediment Mo isotope composition in both directions (towards more negative values initially, but as the ambient seawater progressively shifted to a

more positive composition sediments formed in contact with this evolved seawater would also record a positive shift). For this reason we chose an average of the euxinic samples as the best estimate for the contemporaneous seawater Mo isotope composition.

The THF dataset yields a seawater  $\delta^{98}\text{Mo}$  value of  $+0.32 \pm 0.58$  permil (1SD), which is indistinguishable within uncertainty from the modern riverine flux, and suggests a limited influence on  $\delta^{98}\text{Mo}_{\text{SW}}$  value by adsorption and subsequent burial of Mo in association with Mn- and Fe-oxyhydroxides in oxic and suboxic to anoxic deep-water settings. Critically, since Mo burial efficiencies are low in oxic environments, oxic conditions could have been relatively common at this time, but their influence over the seawater  $\delta^{98}\text{Mo}$  value was yet negligible. The large range of Mo isotope values for euxinic samples from the THF of  $-0.34$  to  $+1.25$  permil implies a dynamic Mo redox cycle and, possibly, a small seawater Mo reservoir. The S isotope composition of pyrite in the THF indicates the presence of oxygen in the upper part of the atmosphere, significant oxidative weathering of crustal sulfides, and a growing seawater sulfate reservoir (Bekker and others, 2004; Scott and others, 2014). At the same time, Mo concentrations and Mo/TOC ratios in the euxinic facies of the THF are larger than the average Archean values for the same facies (typical Archean euxinic black shale Mo concentrations are  $<5$  ppm; Scott and others, 2008). From these parameters, we infer a riverine Mo delivery to the ocean under at least a moderately oxidizing atmosphere with a deep ocean still characterized by widespread anoxia. It is plausible that massive weathering of continental sulfides in association with the GOE (compare Konhauser and others, 2011; Bekker and Holland, 2012) enhanced sulfate delivery to the oceans and was an important mechanism for maintaining widespread euxinic conditions on continental margins at this time, providing an efficient sink for fluvially delivered Mo in relatively shallow-marine settings. The large variation in Mo concentration and isotope composition observed even in euxinic black shales suggests varying sulfide concentration in the water column, which resulted in episodic non-quantitative removal of Mo to the sediments with low  $\delta^{98}\text{Mo}$  values, driving the seawater  $\delta^{98}\text{Mo}$  value to be more positive, which in turn gave rise to more positive  $\delta^{98}\text{Mo}$  values observed in the sediments of the THF.

During the peak of the Lomagundi Event, we estimate a  $\delta^{98}\text{Mo}_{\text{SW}}$  value of  $+1.23 \pm 0.36$  permil (1STD), based on the average isotopic composition of euxinic intervals in the SAF and assuming no fractionation between authigenic Mo and coeval seawater. This represents a significant isotopic enrichment of seawater relative to the assumed combined fluxes with a Mo isotope composition of about  $+0.5$  permil and also relative to the estimated  $\delta^{98}\text{Mo}_{\text{SW}}$  value for the THF. In combination with previous discussion, this increase in the  $\delta^{98}\text{Mo}_{\text{SW}}$  value clearly implies an expansion of suboxic-anoxic and, even oxic conditions.

Next, in the aftermath of the Lomagundi Event, the  $\delta^{98}\text{Mo}_{\text{SW}}$  value decreased to  $+0.70 \pm 0.21$  permil, based on the isotopic composition of euxinic shales from the UZF. The decreased seawater Mo isotope value relative to the SAF reflects a contraction of suboxic-anoxic and oxic depositional environments and an expansion of strongly euxinic settings. Our  $\delta^{98}\text{Mo}_{\text{SW}}$  value for the UZF is largely in agreement with the previous estimate for the same unit by Asael and others (2013). At the same time, we also observe a recovery of the Mo concentrations in these black shales (relative to the SAF) to typical values for the Proterozoic (Scott and others, 2008).

In the previous section, we discussed why under ideal conditions and with an isotopically and quantitatively invariable Mo input flux an increase in the  $\delta^{98}\text{Mo}_{\text{SW}}$  value is expected to be accompanied by an increase in Mo concentrations. However, in our data we see an opposite trend, in which the highest  $\delta^{98}\text{Mo}_{\text{SW}}$  value is observed in the SAF where we also see the lowest Mo concentrations. This difference suggests that the Mo concentrations in our euxinic shales were not solely controlled by the relative

size of the different Mo sinks as linked to ocean redox state. Low seawater Mo concentrations together with high  $\delta^{98}\text{Mo}$  values may represent enhanced trapping of Mo under weakly euxinic conditions where Mo is not quantitatively removed and isotopically fractionated.

In order to further test this hypothesis, we adjusted the fractionation factors as discussed above (that is, mildly euxinic conditions and non-quantitative Mo removal in euxinic settings where removal of Mo is very efficient) to account for a higher  $\delta^{98}\text{Mo}_{\text{SW}}$  value associated with a larger global Mo burial efficiency. The adjusted fractionation factors may partially account for the observed trends (fig. 5). Taking into account the high relative burial rate of organic carbon during the Lomagundi Event, it is plausible that high organic carbon loading across the oceans led to weakly euxinic conditions in a largely anoxic-ferruginous ocean. Under these conditions and in combination with locally developed nutrient limitation oscillating redox conditions would be common in the oceans. In contrast to situations when euxinia develops in silled basins, we infer that on continental margins relatively high burial rates of organic carbon accompanied by anoxia and euxinia would limit extensive and persistent accumulation of high levels of  $\text{H}_2\text{S}$  in the water column.

The pattern of the Mo concentrations in the three units might also reflect changes in the Mo riverine input flux. The high Mo concentrations observed in the THF likely reflect substantial continental sulfide weathering due to the rapid rise in atmospheric oxygen level in association with the GOE. The SAF was deposited more than 150 Ma after this initial pulse of sulfide weathering products when sulfide availability on the continents, and, as a result, the Mo riverine input decreased (Bachan and Kump, 2015). The UZF samples show an increase in Mo concentrations, possibly due to widespread recycling of Mo-enriched sediments (such as the organic matter-rich shales deposited during the GOE), which may have occurred for the first time in Earth's history (compare Kump and others, 2011 and Bekker and Holland, 2012). It should be noted that even though the SAF sediments show low Mo concentrations (average  $[\text{Mo}] = 6.3 \pm 9.0$  ppm), these values are still well above that of average continental crust ( $[\text{Mo}] \approx 1$  ppm for continental crust; Taylor and McLennan (1995)), and therefore weathering of these sediments can contribute substantially to the recovery of Mo in seawater.

As discussed above, our modeling indicates that the balance between suboxic-anoxic and fully euxinic sinks controlled much of the Mo inventory and its isotope composition, at least until the deep ocean became oxygenated in the Phanerozoic. Plotted on the model figures, the  $\delta^{98}\text{Mo}_{\text{SW}}$  values from the THF, UZF, and SAF sections (shaded areas on fig. 4B and fig. 5B) represent slightly different  $A_E/A_S$  ratios, but hold very little information regarding the extent of oxic conditions. There is independent evidence for the growth of the seawater sulfate reservoir during the GOE (in the time between deposition of the THF and SAF; Bekker and others, 2004; Planavsky and others, 2012a; Bekker and Holland, 2012; Scott and others, 2014), reflecting low rates of pyrite burial under more oxygenated seawater conditions, and high organic carbon loading into sediments during the Lomagundi Event, resulting in significant oxygen release to surface environments. Considering the above, it is most parsimonious to infer that the extent of euxinic conditions during deposition of the SAF was limited by the expansion of oxic shallow-water and suboxic-anoxic deep-water conditions. We therefore propose that the observed pattern of Mo isotope values and concentrations indicates that before and during deposition of the THF (*ca.* 2.32 Ga), the oceans were largely anoxic with locally developed euxinic areas. By *ca.* 2.15 Ga when the SAF was deposited, strongly euxinic conditions became rare at the expanse of widespread weakly euxinic settings in which removal of Mo to the sediments in pore waters was non-quantitative. By *ca.* 2.06 Ga when the UZF was deposited, the oceans switched to a



new state with anoxic-suboxic deep-waters and locally developed strongly euxinic conditions in upwelling zones and intracratonic basins.

It is also reasonable to assume that after the Lomagundi Event, the isotopic composition of the Mo input to the ocean was more positive because of exposure and weathering of black shales with higher  $\delta^{98}\text{Mo}$  values on the continents. In this case the shift between the seawater value and the input becomes smaller, implying an even smaller extent of Mo-fractionating environments (that is suboxic-anoxic and oxic settings). For example, if we use a value of 0.7 permil (closer to the average modern fluvial input; Archer and Vance, 2008) for the average post-GOE Mo input instead of 0.5 permil,  $\delta^{98}\text{Mo}$  contour lines on figure 4 will shift by 0.2 permil up and seawater values would reflect a larger extent of euxinia. For the UZF, this would imply a greater fall in seawater oxygen level right after the Lomagundi Event.

The  $\delta^{98}\text{Mo}_{\text{SW}}$  values for the later part of the Proterozoic (fig. 3) range between +1.0 and +1.2 permil (Kendall and others, 2009, 2011; Dahl and others, 2011). In contrast, the  $\delta^{98}\text{Mo}_{\text{SW}}$  value for the 2.5 Ga ‘whiff’ event ( $+1.39 \pm 0.22\text{‰}$ ; Duan and others, 2010), when atmospheric oxygen most likely did not reach the levels expected for the Lomagundi Event, is nevertheless similar to our value for the SAF, consistent with the Mo isotope composition of seawater across the GOE being largely decoupled from atmospheric oxygen level and rather reflecting the extent of suboxic-anoxic settings. Scott and others (2014) made a similar argument for S isotope composition of seawater by comparing pyrite S isotope systematics during and after the Lomagundi Event. Together, these observations suggest a strong coupling between the S and Mo cycles in the Paleoproterozoic.

#### CONCLUSIONS

The Mo isotope composition of early Paleoproterozoic black shales provides evidence for dramatic changes in the redox state and composition of the global ocean in the aftermath of the pervasively anoxic Archean. During the early stage of the GOE, at *ca.* 2.32 Ga, we observe a dynamic oceanic Mo cycle, likely caused by highly variable atmospheric oxygen levels and an enhanced Mo riverine flux into the ocean at a time when massive weathering of continental sulfides occurred for the first time in Earth’s history. The studied organic matter-rich shales record large variations in Mo isotope composition, which were likely produced under variable sulfide concentrations in the water column.

At *ca.* 2.15 Ga, in the middle of the Lomagundi Event, atmospheric oxygen levels stabilized, seawater sulfate concentrations peaked, extensive burial of organic matter occurred, and seawater Mo concentrations decreased. The oceans were largely anoxic with extensively developed, weakly euxinic conditions beneath oxic surface waters. In the immediate aftermath of the Lomagundi Event, we observe the lowest known  $\delta^{98}\text{Mo}_{\text{SW}}$  values after the GOE, supporting previous evidence for a crash in atmospheric and oceanic oxygen levels. Recycling of the organic matter-rich sediments deposited during the Lomagundi Event likely took place, enhancing the Mo supply to the oceans with supracrustal values. Euxinic conditions during this interval were likely limited to intracratonic basins and zones of upwelling on continental margins, where high level of hydrogen sulfide accumulated, whereas the deep ocean remained in a low redox state for the following billion years of Earth’s history.

#### ACKNOWLEDGMENTS

We thank E. Ponzevera, Y. Germain, S. Cheron, A. Boissier, and Steve Bates for technical assistance. This work was supported by IFREMER and funding from Labex Mer (ANR-10-LABX-19-01), NSF (#0820676) and Europole Mer. A.B. acknowledges support from NSF grant EAR-05-45484, NASA Astrobiology Institute Award NNA04CC09A, and an NSERC Discovery and Accelerator Grants. P. Medvedev from

the Institute of Geology, Karelian Research Center, Russia is thanked for arranging access to the UZF samples. The NASA Exobiology and Astrobiology programs provided funds to TWL. We acknowledge Clint Scott (USGS) for his help and various contributions to this paper.

## REFERENCES

- Algeo, T. J., and Lyons, T.W., 2006, Mo-total organic carbon covariation in modern anoxic marine environments: Implications for analysis of paleoredox and paleohydrographic conditions: *Paleoceanography and Paleoclimatology*, v. 21, n. 1, <https://doi.org/10.1029/2004PA001112>
- Anbar, A. D., Duan, Y., Lyons, T. W., Arnold, G. L., Kendall, B., Creaser, R. A., Kaufman, A. J., Gordon, G. W., Scott, C. T., Garvin, J., and Buick, R., 2007, A whiff of oxygen before the great oxidation event?: *Science*, v. 317, n. 5846, p. 1903–1906, <https://doi.org/10.1126/science.1140325>
- Archer, C., and Vance, D., 2008, The isotopic signature of the global riverine molybdenum flux and anoxia in the ancient oceans: *Nature Geoscience*, v. 1, n. 9, p. 597–600, <https://doi.org/10.1038/ngeo282>
- Arnold, G. L., Anbar, A. D., Barling, J., and Lyons, T. W., 2004, Molybdenum isotope evidence for widespread anoxia in mid-Proterozoic oceans: *Science*, v. 304, n. 5667, p. 87–90, <https://doi.org/10.1126/science.1091785>
- Asael, D., Tissot, F. L. H., Reinhard, C. T., Rouxel, O. J., Dauphas, N., Lyons, T. W., Ponzevera, E., Liorzou, C., and Chéron, S., 2013, Coupled molybdenum, iron and uranium stable isotopes as oceanic paleoredox proxies during the Paleoproterozoic Shunga Event: *Chemical Geology*, v. 362, p. 193–210, <https://doi.org/10.1016/j.chemgeo.2013.08.003>
- Bachan, A., and Kump, L. R., 2015, The rise of oxygen and siderite oxidation during the Lomagundi Event: *Proceedings of the National Academy of Sciences of the United States of America*, v. 112, n. 21, p. 6562–6567, <http://doi.org/10.1073/pnas.1422319112>
- Barling, J., and Anbar, A. D., 2004, Molybdenum isotope fractionation during adsorption by manganese oxides: *Earth and Planetary Science Letters*, v. 217, n. 3–4, p. 315–329, [http://doi.org/10.1016/S0012-821X\(03\)00608-3](http://doi.org/10.1016/S0012-821X(03)00608-3)
- Barling, J., Arnold, G. L., and Anbar, A. D., 2001, Natural mass-dependent variations in the isotopic composition of molybdenum: *Earth and Planetary Science Letters*, v. 193, n. 3–4, p. 447–457, [http://doi.org/10.1016/S0012-821X\(01\)00514-3](http://doi.org/10.1016/S0012-821X(01)00514-3)
- Bekker, A., 2014a, Great Oxygenation Event, in *Encyclopedia of Astrobiology*: Berlin, Germany, Springer-Verlag, p. 1–9, [https://doi.org/10.1007/978-3-642-27833-4\\_1752-4](https://doi.org/10.1007/978-3-642-27833-4_1752-4)
- 2014b, Lomagundi Carbon Isotope Excursion, in *Encyclopedia of Astrobiology*: Berlin, Germany, Springer-Verlag, p. 1–6, [https://doi.org/10.1007/978-3-642-27833-4\\_5127-1](https://doi.org/10.1007/978-3-642-27833-4_5127-1)
- Bekker, A., and Holland, H. D., 2012, Oxygen overshoot and recovery during the early Paleoproterozoic: *Earth and Planetary Science Letters*, v. 317–318, p. 295–304, <https://doi.org/10.1016/j.epsl.2011.12.012>
- Bekker, A., Holland, H. D., Wang, P.-L., Rumble III, D., Stein, H. J., Hannah, J. L., Coetsee, L. L., and Beukes, N. J., 2004, Dating the rise of atmospheric oxygen: *Nature*, v. 427, p. 117–20, <https://doi.org/10.1038/nature02260>
- Bekker, A., Holmden, C., Beukes, N. J., Kenig, F., Eglinton, B., and Patterson, W. P., 2008, Fractionation between inorganic and organic carbon during the Lomagundi (2.22–2.1 Ga) carbon isotope excursion: *Earth and Planetary Science Letters*, v. 271, p. 278–291, <https://doi.org/10.1016/j.epsl.2008.04.021>
- Berner, R. A., 1970, Sedimentary Pyrite Formation: *American Journal of Science*, v. 268, n. 1, p. 1–23, <https://doi.org/10.2475/ajs.268.1.1>
- Cameron, E. M., 1982, Sulphate and sulphate reduction in early Precambrian oceans: *Nature*, v. 296, p. 145–148, <https://doi.org/10.1038/296145a0>
- Canfield, D. E., 1998, A new model for Proterozoic ocean chemistry: *Nature*, v. 396, p. 450–453, <https://doi.org/10.1038/24839>
- Canfield, D. E., Raiswell, R., Westrich, J. J. T., Reaves, C. M., and Berner, R. A., 1986, The use of chromium reduction in the analysis of reduced inorganic sulfur in sediments and shales: *Chemical Geology*, v. 54, n. 1–2, p. 149–155, [https://doi.org/10.1016/0009-2541\(86\)90078-1](https://doi.org/10.1016/0009-2541(86)90078-1)
- Canfield, D. E., Raiswell, R., and Bottrell, S., 1992, The reactivity of sedimentary iron minerals toward sulfide: *American Journal of Science*, v. 292, n. 9, p. 659–683, <https://doi.org/10.2475/ajs.292.9.659>
- Canfield, D. E., Ngombi-Pemba, L., Hammarlund, E. U., Bengtson, S., Chaussidon, M., Gauthier-Lafaye, F., Meunier, A., Riboulleau, A., Rollion-Bard, C., Rouxel, O. J., Asael, D., Pierson-Wickmann, A.-C., and El Albani, A., 2013, Oxygen dynamics in the aftermath of the Great Oxidation of Earth's atmosphere: *Proceedings of the National Academy of Sciences of the United States of America*, v. 110, n. 42, p. 16736–16741, <https://doi.org/10.1073/pnas.1315570110>
- Chandler, F. W., 1980, Proterozoic redbed sequences of Canada: *Canadian Geological Survey Bulletin*, v. 311, 53 p., <https://doi.org/10.4095/106239>
- Cloud, P. E., 1968, Atmospheric and Hydrospheric Evolution on the Primitive Earth: Both secular accretion and biological and geochemical processes have affected earth's volatile envelope: *Science*, v. 160, p. 729–736, <https://doi.org/10.1126/science.160.3829.729>
- Coetsee, L. L., Beukes, N. J., Gutzmer, J., and Kakegawa, T., 2006, Links of organic carbon cycling and burial to depositional depth gradients and establishment of a snowball Earth at 2.3 Ga. Evidence from the Timeball Hill Formation, Transvaal Supergroup, South Africa: *South African Journal of Geology*, v. 109, n. 1–2, p. 109–122, <https://doi.org/10.2113/gssajg.109.1-2.109>
- Cumming, V. M., Poulton, S. W., Rooney, A. D., and Selby, D., 2013, Anoxia in the terrestrial environment during the late Mesoproterozoic: *Geology*, v. 41, n. 5, p. 583–586, <http://doi.org/10.1130/G34299.1>

- Dahl, T. W., Canfield, D. E., Rosing, M. T., Frei, R. E., Gordon, G. W., Knoll, A. H., and Anbar, A. D., 2011, Molybdenum evidence for expansive sulfidic water masses in ~750 Ma oceans: Earth and Planetary Science Letters, v. 311, n. 3–4, p. 264–274, <http://doi.org/10.1016/j.epsl.2011.09.016>
- Duan, Y., Anbar, A. D., Arnold, G. L., Lyons, T. W., Gordon, G. W., and Kendall, B., 2010, Molybdenum isotope evidence for mild environmental oxygenation before the Great Oxidation Event: *Geochimica et Cosmochimica Acta*, v. 74, n. 23, p. 6655–6668, <http://doi.org/10.1016/j.gca.2010.08.035>
- Farquhar, J., Zerkle, A. L., and Bekker, A., 2014, Geological and Geochemical Constraints on Earth's Early Atmosphere: *Treatise of Geochemistry*, Elsevier, v. 6, p. 91–138, <https://doi.org/10.1016/B978-0-08-095975-7.01304-8>
- Goldberg, T., Archer, C., Vance, D., and Poulton, S. W., 2009, Mo isotope fractionation during adsorption to Fe (oxyhydr)oxides: *Geochimica et Cosmochimica Acta*, v. 73, n. 21, p. 6502–6516, <https://doi.org/10.1016/j.gca.2009.08.004>
- Gumsley, A. P., Chamberlain, K. R., Bleeker, W., Söderlund, U., de Kock, M. O., Larsson, E. R., and Bekker, A., 2017, Timing and tempo of the Great Oxidation Event: Proceedings of the National Academy of Sciences of the United States of America, v. 114, n. 8, p. 1811–1816, <https://doi.org/10.1073/pnas.1608824114>
- Hannah, J. L., Bekker, A., Stein, H. J., Markey, R. J., and Holland, H. D., 2004, Primitive Os and 2316 Ma age for marine shale: Implications for Paleoproterozoic glacial events and the rise of atmospheric oxygen: Earth and Planetary Science Letters, v. 225, n. 1–2, p. 43–52, <https://doi.org/10.1016/j.epsl.2004.06.013>
- Holland, H. D., 2002, Volcanic gases, black smokers, and the Great Oxidation Event: *Geochimica et Cosmochimica Acta*, v. 66, n. 21, p. 3811–3826, [https://doi.org/10.1016/S0016-7037\(02\)00950-X](https://doi.org/10.1016/S0016-7037(02)00950-X)
- Kendall, B., Creaser, R. A., Gordon, G. W., and Anbar, A. D., 2009, Re–Os and Mo isotope systematics of black shales from the Middle Proterozoic Velkerri and Wollgorang Formations, McArthur Basin, northern Australia: *Geochimica et Cosmochimica Acta*, v. 73, n. 9, p. 2534–2558, <https://doi.org/10.1016/j.gca.2009.02.013>
- Kendall, B., Gordon, G. W., Poulton, S. W., and Anbar, A. D., 2011, Molybdenum isotope constraints on the extent of late Paleoproterozoic ocean euxinia: Earth and Planetary Science Letters, v. 307, n. 3–4, p. 450–460, <https://doi.org/10.1016/j.epsl.2011.05.019>
- Kipp, M. A., Stüeken, E. E., Bekker, A., and Buick, R., 2017, Selenium isotopes record extensive marine suboxia during the Great Oxidation Event: Proceedings of the National Academy of Sciences of the United States of America, v. 114, n. 5, p. 875–880, <https://doi.org/10.1073/pnas.1615867114>
- Konhäuser, K. O., Lalonde, S. V., Planavsky, N. J., Pecoits, E., Lyons, T. W., Mojzsis, S. J., Rouxel, O. J., Barley, M. E., Rosiere, C., Fralick, P. W., Kump, L. R., and Bekker, A., 2011, Aerobic Pyrite Oxidation and Acid Rock Drainage During the Great Oxidation Event: *Nature*, v. 478, p. 369–373, <https://doi.org/10.1038/nature10511>
- Kump, L. R., Junium, C., Arthur, M. A., Brasier, A., Fallick, A., Melezhik, V., Lepland, A., Crne, A. E., and Luo, G., 2011, Isotopic evidence for massive oxidation of organic matter following the great oxidation event: *Science*, v. 334, n. 6063, p. 1694–1696, <https://doi.org/10.1126/science.1213999>
- Lehmann, B., Nägler, T. F., Holland, H. D., Wille, M., Mao, J., Pan, J., Ma, D., and Dulski, P., 2007, Highly metalliferous carbonaceous shale and Early Cambrian seawater: *Geology*, v. 35, n. 5, p. 403–406, <https://doi.org/10.1130/G23543A.1>
- Luo, G., Ono, S., Beukes, N. J., Wang, D. T., Xie, S., and Summons, R. E., 2016, Rapid oxygenation of Earth's atmosphere 2.33 billion years ago: *Science Advances*, v. 2, n. 5, 9 p., <https://doi.org/10.1126/sciadv.1600134>
- Lyons, T. W., Reinhard, C. T., and Planavsky, N. J., 2014, The rise of oxygen in Earth's early ocean and atmosphere: *Nature*, v. 506, p. 307–15, <https://doi.org/10.1038/nature13068>
- Melezhik, V., and Fallick, A., 1999, Extreme  $^{13}\text{C}_{\text{carb}}$  enrichment in ca. 2.0 Ga magnesite–stromatolite–dolomite–“red beds” association in a global context: A case for the world-wide signal enhanced by a local environment: *Earth-Science Reviews*, v. 48, n. 1–2, 71–120, [https://doi.org/10.1016/S0012-8252\(99\)000446](https://doi.org/10.1016/S0012-8252(99)000446)
- Nägler, T. F., Neubert, N., Böttcher, M. E., Dellwig, O., and Schnetger, B., 2011, Molybdenum isotope fractionation in pelagic euxinia: Evidence from the modern Black and Baltic Seas: *Chemical Geology*, v. 289, n. 1–2, p. 1–11, <https://doi.org/10.1016/j.chemgeo.2011.07.001>
- Nägler, T. F., Anbar, A. D., Archer, C., Goldberg, T., Gordon, G. W., Greber, N. D., Siebert, C., Sohrin, Y., and Vance, D., 2014, Proposal for an International Molybdenum Isotope Measurement Standard and Data Representation: *Geostandards and Geoanalytical Research*, v. 38, n. 2, p. 149–151, <https://doi.org/10.1111/j.1751-908X.2013.00275.x>
- Neubert, N., Nägler, T. F., and Böttcher, M. E., 2008, Sulfidity controls molybdenum isotope fractionation into euxinic sediments: Evidence from the modern Black Sea: *Geology*, v. 36, n. 10, p. 775–778, <https://doi.org/10.1130/G24959A.1>
- Olson, S. L., Kump, L. R., and Kasting, J. F., 2013, Quantifying the areal extent and dissolved oxygen concentrations of Archean oxygen oases: *Chemical Geology*, v. 362, p. 35–43, <http://doi.org/10.1016/j.chemgeo.2013.08.012>
- Ossa Ossa, F., Eickmann, B., Hofmann, A., Planavsky, N. J., Asael, D., Pambo, F., and Bekker, A., 2018, Two-step deoxygenation at the end of the Paleoproterozoic Lomagundi Event: *Earth and Planetary Science Letters*, v. 486, p. 70–83, <https://doi.org/10.1016/j.epsl.2018.01.009>
- Partin, C. A., Bekker, A., Planavsky, N. J., Scott, C. T., Gill, B. C., Li, C., Podkovyrov, V., Maslov, A., Konhäuser, K. O., Lalonde, S. V., Love, G. D., Poulton, S. W., and Lyons, T. W., 2013a, Large-scale fluctuations in Precambrian atmospheric and oceanic oxygen levels from the record of U in shales: *Earth and Planetary Science Letters*, v. 369–370, p. 284–293, <http://doi.org/10.1016/j.epsl.2013.03.031>
- Partin, C. A., Lalonde, S. V., Planavsky, N. J., Bekker, A., Rouxel, O. J., Lyons, T. W., and Konhäuser, K. O.,

- 2013b, Uranium in iron formations and the rise of atmospheric oxygen: *Chemical Geology*, v. 362, p. 82–90, <http://doi.org/10.1016/j.chemgeo.2013.09.005>
- Pavlov, A. A., and Kasting, J. F., 2002, Mass-independent fractionation of sulfur isotopes in Archean sediments: Strong evidence for an anoxic Archean atmosphere: *Astrobiology*, v. 2, n. 1, p. 27–41, <http://doi.org/10.1089/153110702753621321>
- Planavsky, N. J., McGoldrick, P., Scott, C. T., Li, C., Reinhard, C. T., Kelly, A. E., Chu, X., Bekker, A., Love, G. D., and Lyons, T. W., 2011, Widespread iron-rich conditions in the mid-Proterozoic ocean: *Nature*, v. 477, p. 448–451, <http://doi.org/10.1038/nature10327>
- Planavsky, N. J., Bekker, A., Hofmann, A., Owens, J. D., and Lyons, T. W., 2012a, Sulfur record of rising and falling marine oxygen and sulfate levels during the Lomagundi event: *Proceedings of the National Academy of Sciences of the United States of America*, v. 109, p. 18300–18305, <http://doi.org/10.1073/pnas.1120387109>
- Planavsky, N. J., Rouxel, O. J., Bekker, A., Hofmann, A., Little, C. T. S., and Lyons, T. W., 2012b, Iron isotope composition of some Archean and Proterozoic iron formations: *Geochimica et Cosmochimica Acta*, v. 80, p. 158–169, <http://doi.org/10.1016/j.gca.2011.12.001>
- Planavsky, N., Partin, C., and Bekker, A., 2014, Carbon Isotopes as a Geochemical Tracer, *in* *Encyclopedia of Astrobiology*: Berlin, Springer-Verlag, p. 1–6, [https://doi.org/10.1007/978-3-642-27833-4\\_228-2](https://doi.org/10.1007/978-3-642-27833-4_228-2)
- Poulson, R. L., Siebert, C., McManus, J., and Berelson, W. M., 2006, Authigenic molybdenum isotope signatures in marine sediments: *Geology*, v. 34, n. 8, p. 617–620, <https://doi.org/10.1130/G22485.1>
- Poulson Brucker, R., McManus, J., Severmann, S., Owens, J., and Lyons, T. W., 2011, Trace metal enrichments in Lake Tanganyika sediments: Controls on trace metal burial in lacustrine systems: *Geochimica et Cosmochimica Acta*, v. 75, n. 2, p. 483–499, <https://doi.org/10.1016/j.gca.2010.09.041>
- Poulson Brucker, R. L., McManus, J., Severmann, S., and Berelson, W. M., 2009, Molybdenum behavior during early diagenesis: Insights from Mo isotopes: *Geochemistry, Geophysics, Geosystems*, v. 10, n. 6, Q06010, <https://doi.org/10.1029/2008GC002180>
- Poulton, S. W., and Canfield, D. E., 2005, Development of a sequential extraction procedure for iron: Implications for iron partitioning in continentally derived particulates: *Chemical Geology*, v. 214, n. 3–4, p. 209–221, <https://doi.org/10.1016/j.chemgeo.2004.09.003>
- 2011, Ferruginous Conditions: A Dominant Feature of the Ocean through Earth's History: *Elements*, v. 7, n. 2, p. 107–112, <https://doi.org/10.2113/gselements.7.2.107>
- Poulton, S. W., Krom, M. D., and Raiswell, R., 2004, A revised scheme for the reactivity of iron (oxyhydr)oxide minerals towards dissolved sulfide: *Geochimica et Cosmochimica Acta*, v. 68, n. 18, p. 3703–3715, <https://doi.org/10.1016/j.gca.2004.03.012>
- Poulton, S. W., Fralick, P. W., and Canfield, D. E., 2010, Spatial variability in oceanic redox structure 1.8 billion years ago: *Nature Geoscience*, v. 3, p. 486–490, <https://doi.org/10.1038/ngeo889>
- Raiswell, R., Canfield, D. E., and Berner, R. A., 1994, A comparison of iron extraction methods for the determination of degree of pyritisation and the recognition of iron-limited pyrite formation: *Chemical Geology*, v. 111, n. 1–4, p. 101–110, [https://doi.org/10.1016/0009-2541\(94\)90084-1](https://doi.org/10.1016/0009-2541(94)90084-1)
- Raiswell, R., Reinhard, C. T., Derkowski, A., Owens, J., Bottrell, S. H., Anbar, A. D., and Lyons, T. W., 2011, Formation of syngenetic and early diagenetic iron minerals in the late Archean Mt. McRae Shale, Hamersley Basin, Australia: New insights on the patterns, controls and paleoenvironmental implications of authigenic mineral formation: *Geochimica et Cosmochimica Acta*, v. 75, n. 4, p. 1072–1087, <https://doi.org/10.1016/j.gca.2010.11.013>
- Rasmussen, B., Fletcher, I. R., Bekker, A., Muhling, J. R., Gregory, C. J., and Thorne, A. M., 2012, Deposition of 1.88-billion-year-old iron formations as a consequence of rapid crustal growth: *Nature*, v. 484, p. 498–501, <https://doi.org/10.1038/nature11021>
- Reinhard, C. T., Raiswell, R., Scott, C., Anbar, A. D., and Lyons, T. W., 2009, A late Archean sulfidic sea stimulated by early oxidative weathering of the continents: *Science*, v. 326, n. 5953, p. 713–716, <https://doi.org/10.1126/science.1176711>
- Reinhard, C. T., Planavsky, N. J., and Lyons, T. W., 2013, Long-term sedimentary recycling of rare sulphur isotope anomalies: *Nature*, v. 497, p. 100–103, <https://doi.org/10.1038/nature12021>
- Roscoe, S. M., 1969, Huronian rocks and uraniferous conglomerates in the Canadian Shield: *Geological Survey of Canada, Paper n. 68–40*, 217 p., <https://doi.org/10.4095/102290>
- Rouxel, O. J., Bekker, A., and Edwards, K. J., 2005, Iron isotope constraints on the Archean and Paleoproterozoic ocean redox state: *Science*, v. 307, n. 5712, p. 1088–1091, <https://doi.org/10.1126/science.1105692>
- Scott, C., and Lyons, T. W., 2012, Contrasting molybdenum cycling and isotopic properties in euxinic versus non-euxinic sediments and sedimentary rocks: Refining the paleoproxies: *Chemical Geology*, v. 324–325, p. 19–27, <https://doi.org/10.1016/j.chemgeo.2012.05.012>
- Scott, C., Lyons, T. W., Bekker, A., Shen, Y., Poulton, S. W., Chu, X., and Anbar, A. D., 2008, Tracing the stepwise oxygenation of the Proterozoic ocean: *Nature*, v. 452, p. 456–459, <https://doi.org/10.1038/nature06811>
- Scott, C., Wing, B. A., Bekker, A., Planavsky, N. J., Medvedev, P., Bates, S. M., Yun, M., and Lyons, T. W., 2014, Pyrite multiple-sulfur isotope evidence for rapid expansion and contraction of the early Paleoproterozoic seawater sulfate reservoir: *Earth and Planetary Science Letters*, v. 389, p. 95–104, <https://doi.org/10.1016/j.epsl.2013.12.010>
- Siebert, C., Nägler, T. F., and Kramers, J. D., 2001, Determination of molybdenum isotope fractionation by double-spike multicollector inductively coupled plasma mass spectrometry: *Geochemistry, Geophysics, Geosystems*, v. 2, n. 7, <https://doi.org/10.1029/2000GC000124>
- Slack, J. F., and Cannon, W. F., 2009, Extraterrestrial demise of banded iron formations 1.85 billion years ago: *Geology*, v. 37, n. 11, p. 1011–1014, <https://doi.org/10.1130/G30259A.1>

- Taylor, S. R., and McLennan, S. M., 1995, The geochemical evolution of the continental crust: Reviews of Geophysics, v. 33, n. 2, p. 241–265, <https://doi.org/10.1029/95RG00262>
- Thomson, D., Rainbird, R. H., Planavsky, N., Lyons, T. W., and Bekker, A., 2015, Chemostratigraphy of the Shaler Supergroup, Victoria Island, NW Canada: A record of ocean composition prior to the Cryogenian glaciations: Precambrian Research, v. 263, p. 232–245, <https://doi.org/10.1016/j.precamres.2015.02.007>
- Tossell, J. A., 2005, Calculating the partitioning of the isotopes of Mo between oxidic and sulfidic species in aqueous solution: Geochimica et Cosmochimica Acta, v. 69, n. 12, p. 2981–2993, <https://doi.org/10.1016/j.gca.2005.01.016>
- Zerle, A. L., Poulton, S. W., Newton, R. J., Mettam, C., Claire, M. W., Bekker, A., and Junium, C. K., 2017, Onset of the aerobic nitrogen cycle during the Great Oxidation Event: Nature, v. 542, p. 465–467, <https://doi.org/10.1038/nature20826>